NASA/TM—2012-217671 AIAA–2012–2087

A Comparison of Combustor-Noise Models

Lennart S. Hultgren
Glenn Research Center, Cleveland, Ohio

August 2012

NASA STI Program . . . in Profile

Since its founding, NASA has been dedicated to the advancement of aeronautics and space science. The NASA Scientific and Technical Information (STI) program plays a key part in helping NASA maintain this important role.

The NASA STI Program operates under the auspices of the Agency Chief Information Officer. It collects, organizes, provides for archiving, and disseminates NASA's STI. The NASA STI program provides access to the NASA Aeronautics and Space Database and its public interface, the NASA Technical Reports Server, thus providing one of the largest collections of aeronautical and space science STI in the world. Results are published in both non-NASA channels and by NASA in the NASA STI Report Series, which includes the following report types:

- TECHNICAL PUBLICATION. Reports of completed research or a major significant phase of research that present the results of NASA programs and include extensive data or theoretical analysis. Includes compilations of significant scientific and technical data and information deemed to be of continuing reference value. NASA counterpart of peer-reviewed formal professional papers but has less stringent limitations on manuscript length and extent of graphic presentations.

- TECHNICAL MEMORANDUM. Scientific and technical findings that are preliminary or of specialized interest, e.g., quick release reports, working papers, and bibliographies that contain minimal annotation. Does not contain extensive analysis.

- CONTRACTOR REPORT. Scientific and technical findings by NASA-sponsored contractors and grantees.

- CONFERENCE PUBLICATION. Collected papers from scientific and technical conferences, symposia, seminars, or other meetings sponsored or cosponsored by NASA.

- SPECIAL PUBLICATION. Scientific, technical, or historical information from NASA programs, projects, and missions, often concerned with subjects having substantial public interest.

- TECHNICAL TRANSLATION. English-language translations of foreign scientific and technical material pertinent to NASA's mission.

Specialized services also include creating custom thesauri, building customized databases, organizing and publishing research results.

For more information about the NASA STI program, see the following:

- Access the NASA STI program home page at *http://www.sti.nasa.gov*

- E-mail your question to *help@sti.nasa.gov*

- Fax your question to the NASA STI Information Desk at 443–757–5803

- Phone the NASA STI Information Desk at 443–757–5802

- Write to:
  STI Information Desk
  NASA Center for AeroSpace Information
  7115 Standard Drive
  Hanover, MD 21076–1320

NASA/TM—2012-217671 AIAA–2012–2087

A Comparison of Combustor-Noise Models

Lennart S. Hultgren
Glenn Research Center, Cleveland, Ohio

Prepared for the
18th Aeroacoustics Conference
cosponsored by the American Institute of Aeronautics and Astronautics and Confederation of European Aerospace Societies
Colorado Springs, Colorado, June 4–6, 2012

National Aeronautics and
Space Administration

Glenn Research Center
Cleveland, Ohio 44135

August 2012

Acknowledgments

This work was supported by the NASA Fundamental Aeronautics Program Subsonic Fixed Wing Project (SFW). The NASA Fundamental Aeronautics Program has the principal objective of overcoming today's national challenges in air transportation. The work herein is aligned with the SFW Reduce-Perceived-Noise Technical Challenge, which aims to enable concepts and technologies to dramatically reduce the perceived aircraft noise outside of airport boundaries. It is part of a NASA-internal and NASA-sponsored external research effort for the development and improvement of aircraft noise-prediction capability and tools. The author thanks Russell W. Claus for providing the existing NPSS simulation mean-line data for the E^3 engine.

This work was sponsored by the Fundamental Aeronautics Program at the NASA Glenn Research Center.

Level of Review: This material has been technically reviewed by technical management.

Available from

NASA Center for Aerospace Information
7115 Standard Drive
Hanover, MD 21076–1320

National Technical Information Service
5301 Shawnee Road
Alexandria, VA 22312

Available electronically at http://www.sti.nasa.gov

A Comparison of Combustor-Noise Models

Lennart S. Hultgren
National Aeronautics and Space Administration
Glenn Research Center
Cleveland, Ohio 44135

The current status of combustor-noise prediction in the NASA Aircraft Noise Prediction Program (ANOPP) for current-generation (N) turbofan engines is summarized. Best methods for near-term updates are reviewed. Long-term needs and challenges for the N+1 through N+3 time frame are discussed. This work was carried out under the NASA Fundamental Aeronautics Program, Subsonic Fixed Wing Project, Quiet Aircraft Subproject.

I. Introduction

The anticipated increase in future air traffic makes further reduction of subsonic transport-aircraft noise an imperative. Currently, noise generated in the jet engine core by components such as the compressor, combustor, and turbine can be significant contributors to the overall noise signature at low-power conditions, typical of approach flight. For existing engines, core noise is typically dominated by jet and fan noise at high engine-power settings during takeoff. However, current design trends and expected technological advances in engine-cycle design as well as noise-reduction methods are likely to increase the relative importance of core noise at all engine-power levels.[1] Consequently, core noise will need to be addressed in order to meet future aircraft noise-reduction goals. In fact, core noise may well set a propulsion-noise floor limiting the effects of future fan and jet noise reduction techniques if not further controlled. The present paper is concerned with combustor noise, which is a low-frequency contributor to the noise generated in the turbofan engine core. It can be a significant aspect of the aft-quadrant overall noise signature at typical approach conditions for today's turbofan engines and it is predicted[1] to make a significant contribution to all certification noise levels for near-future engine designs.

Combustor noise can be of either the direct or indirect type. The noise frequency for either type is set by the unsteady combustion process and the peak value is generally believed to fall in the range of 400–500 Hz. The unsteady combustion process is the source of pressure, entropy, and vorticity fluctuations. A fraction of the pressure disturbances are acoustic pressure fluctuations with the balance being hydrodynamical unsteadiness. The former is what is referred to as direct combustor noise. Its spectrum can be modified by the combustor geometry as well as pressure feedback on the unsteady combustion process itself. The direct combustor noise is reduced due to transmission effects during its propagation through the turbine stages. The combustor entropy (temperature) fluctuations are convected downstream with the local mean velocity and are converted to acoustic pressure fluctuations in the turbine and other regions where flow properties change rapidly. This is the indirect process of turbomachinery combustor-noise generation. This is potentially a very effective mechanism and occurs at all turbine stages. The indirect noise occurs in the same basic frequency range as the direct noise, but their spectral-distribution shapes could be quite different and both are affected by the propagation through the engine core. Figure 1 illustrates the dual paths of combustor noise. Note that the direct and indirect noise contributions are correlated at the source because both are caused by the unsteady heat addition. The relative importance of the two combustor-noise components is still an unresolved issue.[2–7]

Major advances in combustor-noise source modeling occurred during the 1970s and early 1980s and are discussed in the review chapter by Mahan and Karchmer[8] and references therein. Semi-empirical relations that correlate noise levels with engine operating parameters based on full-engine test data were mainly developed by aircraft engine companies, often with support from Department of Transportation/Federal Aviation Administration (DOT/FAA) or National Aeronautics and Space Administration (NASA). Significant development of diagnostic techniques also took place during this time period. However, research resources were generally redirected towards the more pressing

† Associate Fellow AIAA

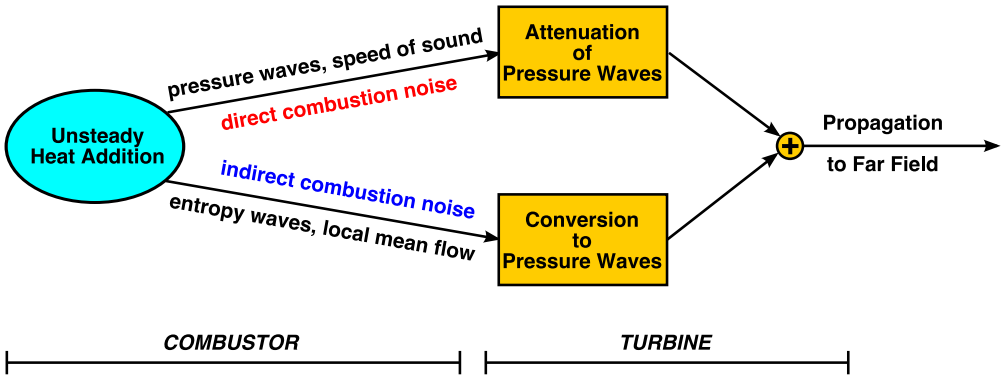

Figure 1. Dual paths for turbofan combustor noise

non-core noise issues in the late 1980s. Combustor noise, consequently, received very limited attention until the early 2000s when reduction techniques for jet and fan noise had further matured to a point, coupled with turbofan design trends, where further noise reduction would require core noise to also be addressed. It was also realized at that time that core noise was an important contributor to airport ramp noise due to auxiliary power units (APU).

Direct measurement of turbofan-engine combustor noise is difficult because of the presence of jet noise in the frequency range of interest. Since flight effects reduce jet noise more than combustor noise, combustor noise can be a significant contributor to aircraft in-flight noise but may be masked by jet noise under the corresponding static-engine test conditions. To overcome this obstacle, researchers[9–23] developed coherence techniques utilizing engine-internal, as well as far-field, measurements to identify the far-field combustor-noise component. Modal analyses[24–29] were also carried out to determine the source and propagation characteristics of combustor noise.

The current paper discusses several semi-empirical models for turbofan combustor noise. The three-spectrum model proposed by Stone et al.[30] for GE turbofan-engine combustor noise will be discussed and compared with ANOPP predictions for several relevant cases. The connection to the work by von Glahn and Krejsa,[31] Karchmer,[24] and Royalty and Schuster[29] will also be discussed.

II. Combustor-Noise Models

Semi-empirical models for the total acoustic power are, in general, developed based on physical considerations with model coefficients/constants determined using isolated-component and static-engine test data. Then the far-field directivity and universal spectral distribution are obtained empirically. In the case of full-engine tests, the measured total far-field acoustic signature normally is adjusted by subtracting the low-frequency jet noise using an appropriate model to reveal the core noise. This represents a weakness since combustor noise is not always a dominant noise source at low engine-power settings.

A. Early Models

Huff et al.[32] reviewed the early 1970s state-of-the-art in engine combustor-noise prediction and recommended an interim semi-empirical method to provide such a capability for the NASA Aircraft Noise Prediction Program (ANOPP).[33,34] The proposed direct-combustor-noise method combined a General Electric[35] developed formula for the total acoustic power as a function of the engine operating condition, a Boeing[36] obtained result for polar directivity, and a single-peak spectral distribution based on the in-flight SAE ARP876[37] jet-noise spectrum. As recommended in the Boeing[36] work, Huff et al.[32] suggested using a fixed peak frequency of 400 Hz. Emmerling et al.[38] improved the General-Electric model by correlating the combustor-noise attenuation by the turbine with the design-point work extraction of the turbine and validated the resulting model using several sets of engine data. Ho and Doyle[39] provided further validation and discussion of this model (see also Mahan and Karchmer[8]). This simple direct combustor-noise model[38,39] still forms the kernel of the ANOPP core-noise module and is referred to therein as the SAE method. The current ANOPP module also contains a small-engine revision[40] of this method (referred to as SmE herein) and an intermediate-narrow-band method[41] to account for tail-pipe resonances.

Also during the latter half of the 1970s, researchers at Pratt & Whitney[5,42] developed a semi-empirical prediction method for direct combustor noise. They derived models for the total acoustic power level, turbine coupling/ trans-

mission losses, and peak frequency; and they empirically determined model constants, the directivity pattern, and a universal normalized spectral distribution using a range of burner-rig and full-scale static engine tests. Mathews et al.[5] also measured the dynamic temperature characteristics at the exit as well as inside of a burner in a rig experiment to provide inputs for an existing Pratt & Whitney indirect combustor noise model.[43] They found experimentally that the unsteady temperature level (roughly 9 % at the exit) depended mainly on the total temperature increase across the burner and that the corresponding length scales were approximately proportional to a burner flow rate parameter. Based on these measurements and the prediction codes, they found that indirect combustor noise should be 18-22 dB lower than direct noise in the absence of turbine attenuation.

There are similarities and differences between the General Electric and Pratt & Whitney direct combustor-noise results (see also discussion in Mahan and Karchmer[8]). In both, the total acoustic power level is proportional to the second power of the combustor pressure and the second power of the temperature rise across the combustor (the Pratt & Whitney model uses the air-fuel ratio which essentially is equivalent to the temperature rise). The combustor mass-flow rate linearly affects the total acoustic power in the General-Electric model, whereas in the Pratt & Whitney formula it enters through a burner-flow parameter to the fourth power. The Pratt & Whitney result also depends on burner-geometry information such as the number of fuel nozzles and the burner cross-sectional area. Their formulas for turbine losses are different but both are frequency independent. The latter fact implies that, in the absence of resonances, measured spectra for burner-rig and full-engine static tests should be quite similar. Furthermore, their directivity patterns are in good agreement and their single-peak universal spectral distributions are similar when frequencies are normalized with the peak frequency. The peak frequency in the General-Electric model is always 400 Hz, but the corresponding Pratt & Whitney formula involves burner design and geometry parameters. In general, each of these prediction tools has shown good agreement with data from the engine manufacturer that developed the method, but not with data from other companies. The need for distinct models may be caused by differences in burner design philosophy.[44] Zuckermann[44] summarized the history and results of the DOT/FAA sponsorship of core-noise research and provided further comments. The report also pointed out the need for continued improvements in turbine-attenuation and indirect combustor-noise source modeling.

B. Current ANOPP Models

For a static-engine test, the (dimensional) combustor-noise mean-square pressure in each 1/3-octave band (b) is given by

$$< p^2 >^{(b)} = \frac{\rho_\infty c_\infty \Pi D(\theta) S(f_b)}{4\pi r_s^2} \tag{1a}$$

for both the SAE and SmE methods in ANOPP, where r_s is the distance between the source and the observer and ρ_∞ and c_∞ are the ambient density and speed of sound. $D(\theta)$ is a directivity function that depends only on the polar angle θ and satisfies the normalization condition

$$\int_0^\pi D(\theta) \sin\theta \mathrm{d}\theta = 2\,. \tag{1b}$$

$S(f_b)$ is a spectrum function satisfying

$$\sum_b S(f_b) = 1 \tag{1c}$$

and f_b is the 1/3-octave-band center frequency. Π is the total acoustic power

$$\Pi = \int_A \frac{\sum_b < p^2 >^{(b)}}{\rho_\infty c_\infty} \mathrm{d}A\,, \tag{1d}$$

where $\mathrm{d}A = r_s^2 \sin\theta \mathrm{d}\theta \mathrm{d}\phi$, with ϕ denoting the azimuthal angle. The sound pressure level $SPL^{(b)}$ in an 1/3-octave frequency band, the overall sound pressure level $OASPL$, and the power level PWL are given by

$$SPL^{(b)} = 10\log(< p^2 >^{(b)} / p_{ref}^2)\,, \tag{2a}$$

$$OASPL = 10\log(\textstyle\sum_b < p^2 >^{(b)} / p_{ref}^2) = 10\log[\rho_\infty c_\infty \Pi D(\theta)/4\pi r_s^2 p_{ref}^2]\,, \tag{2b}$$

$$PWL = 10\log(\Pi/\Pi_{ref})\,, \tag{2c}$$

where $p_{ref} = 2 \times 10^{-5}$ Pa and $\Pi_{ref} = 1 \times 10^{-12}$ W if SI units are used. The ANOPP formula for the total acoustic power is

$$\Pi = 10^{K/10} c_\infty^2 \dot{m}_{core} \left(\frac{T_{t,ce} - T_{t,ci}}{T_{t,ci}} \right)^2 \left(\frac{P_{t,ci}}{P_\infty} \right)^2 \times F_{TA} \,, \tag{3a}$$

where the constant $K = -60.53\ldots$ in the SAE method and $K = -64.53\ldots$ in the SmE method.[a] $\dot{m}_{core}$ is the mass flow rate into the combustor, $T_{t,ci}$ and $T_{t,ce}$ are the total temperature at the combustor inlet and exit, $P_{t,ci}$ is the total combustor-inlet pressure, and P_∞ is the reference (static) pressure. The reference state is ambient conditions, actual or standard sea-level values. F_{TA} is a turbine attenuation, or loss, factor and is given by[35]

$$F_{TA} = \left(\frac{\Delta T_{des}}{T_\infty} \right)^{-4} \,, \tag{3b}$$

where ΔT_{des} is the design-point temperature drop across the turbine and T_∞ is the reference temperature. Note that the acoustic transmission loss is independent of the engine operating condition. Eq. (3b) will be referred to as the ANOPP-GE formula for turbine-transmission loss herein.

In the ANOPP intermediate-narrow-band method,[41] the combustor-noise mean-square pressure, $< p^2 >^{(n)}$, associated with each narrow-band frequency range (n) is given by

$$< p^2 >^{(n)} = \frac{\rho_\infty c_\infty \Pi D(\theta, f_n) S(f_n)}{4\pi r_s^2} \,, \tag{4a}$$

which is analogous to Eq. (1a), but with a directivity function $D(\theta, f_n)$ that now also depends on the narrow-band center frequency, f_n, in addition to the polar angle, and with a spectrum function $S(f_n)$ that also can account for a tail-pipe resonance. The product $D(\theta, f_n)S(f_n)$ satisfies a normalization condition equivalent to Eqs. (1b) and (1c),

$$\int_0^\pi \sum_n D(\theta, f_n) S(f_n) \sin\theta \mathrm{d}\theta = 2 \,. \tag{4b}$$

The total acoustic power is also here given by Eqs. (3a) and (3b). The narrow-band results are then summed up to yield the customary 1/3-octave results in ANOPP, i.e.

$$< p^2 >^{(b)} = \sum_{n \in b} < p^2 >^{(n)} \,. \tag{5}$$

C. Turbine-Transmission-Loss Update

Time-series data obtained from the NASA/Honeywell Engine Validation of Noise and Emission Reduction Technology program[45] (EVNERT) was used by Hultgren[46] to assess the turbine transfer of direct combustor-noise and to recommend an update to the turbine-attenuation formula used in ANOPP. This static-engine test activity was carried out in Honeywell Aerospace's San Tan outdoor facility from 2005 to 2007. The program used the Honeywell TECH977 research engine, which is typical of a business-jet application in the 6,000–8,000 lbs thrust class.

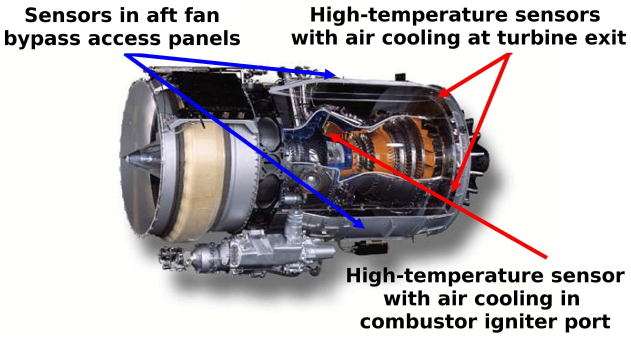

Figure 2. Honeywell TECH977 turbofan engine-internal sensors

The engine-internal instrumentation in one of the many EVNERT test configurations included high-temperature pressure sensors with air cooling located in a combustor ignitor port (one sensor) and at the turbine exit (two sensors), see Fig. 2. The true combustion-noise turbine-transfer function was educed from the EVNERT data by using a three-signal approach. Note that the true turbine gain factor is always underpredicted by a directly measured one, using only two sensors, because of a positive bias error caused by the presence of pressure fluctuations in the combustor that are uncorrelated with the combustor noise.[46] The resulting gain factors were compared with

[a]The SAE and SmE methods differ only by 4 dB in the acoustic power level.

the corresponding constant values obtained from Eq. (3b) and a simplified[8] Pratt & Whitney[5,42] acoustic-turbine-loss formula,

$$F_{TA} = \frac{0.8\zeta}{(1+\zeta)^2}\,, \tag{6}$$

where ζ is the ratio of the characteristic impedances across the turbine, i.e. $\zeta = \rho_{te}c_{te}/\rho_{ti}c_{ti}$ with ρ and c denoting density and speed of sound, respectively, and the subscripts 'te' and 'ti' indicating turbine exit and inlet. Both empirical formulas, (3b) and (6), are frequency independent. Hultgren[46,b] found that the gain factor obtained from the simplified Pratt & Whitney formula (6) agreed better with the experimental results for frequencies of practical importance.

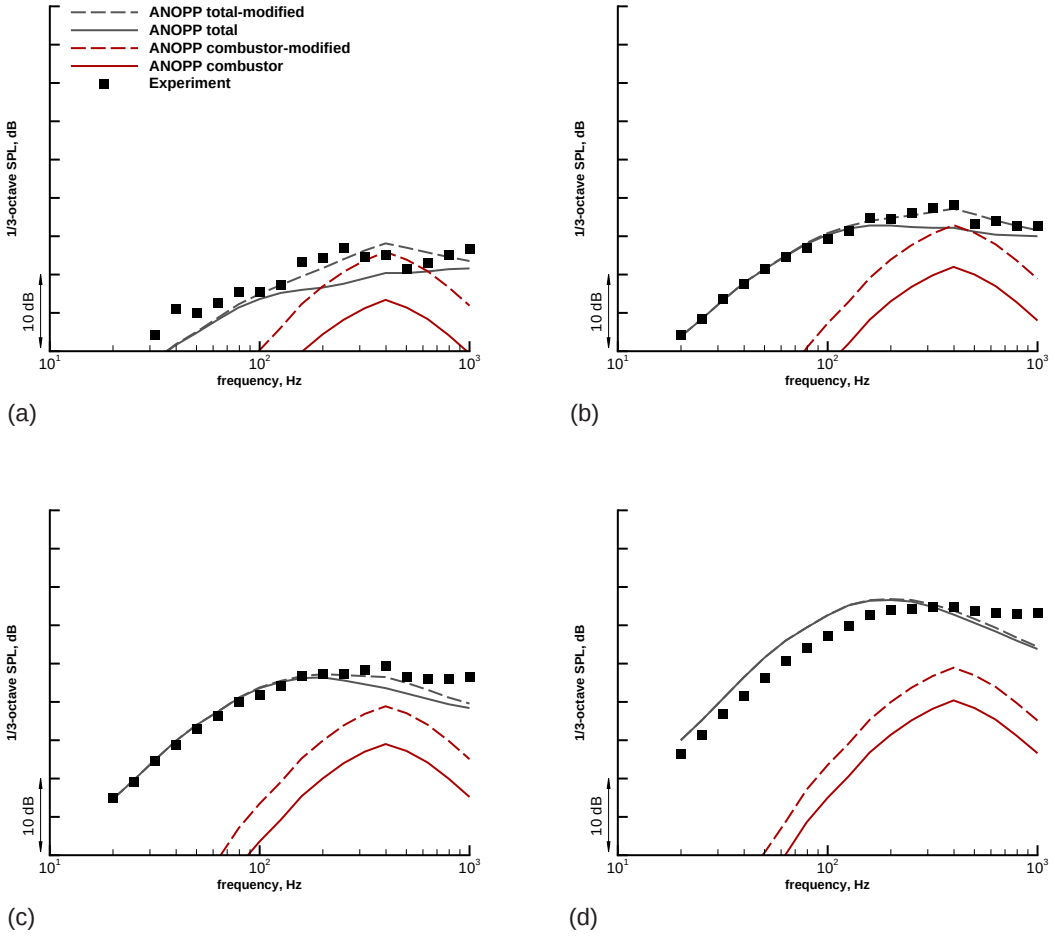

Figure 3. Total and combustor noise 1/3-octave SPL versus 1/3-octave center frequency in the 130^o direction; symbols and solid lines—data and ANOPP predictions from Ref. 23; dashed lines—ANOPP predictions modified to use the P&W turbine-attenuation from Ref. 46; (a): 48 % corrected fan speed (flight idle); (b): 60 % corrected fan speed (approach); (c): 71 % corrected fan speed (cutback); (d): 87 % corrected fan speed (takeoff)

Hultgren[46] reexamined the far-field 1/3-octave *SPL* results in the 130^o direction by Hultgren and Miles,[23] for the same EVNERT dataset as above, by applying a post-correction to the original ANOPP predictions for both the total noise signature and the combustion-noise component. It was found that replacing the ANOPP-GE combustor-noise turbine-attenuation function (3b) with the simplified Pratt & Whitney one (6) clearly improved the total-noise predictions and also improved the combustion-noise predictions. The latter comparison was not as conclusive as the former due to the inherent difficulty in extracting the combustion-noise component from the total noise signature. However, the former would not be true if the combustion-noise component predictions had not been improved by the attenuation-formula change.

[b]Due to a typographical error, the formula in Ref. 46 (Eq. 13) corresponding to Eq. (6) is inverted, but the computations therein are correct.

Figure 3 shows the original[23] far-field results in the 130^o direction as well as the effects[46] on the ANOPP predictions by replacing the ANOPP-GE turbine-attenuation factor by the simplified Pratt & Whitney formula. The 1/3-octave sound-pressure-level (*SPL*) results are shown at the four engine power settings of 48, 60, 71, and 87 percent corrected fan speed (flight-idle, approach, cutback, and takeoff conditions) for the 1/3-octave center frequency range of 20 to 1000 Hz. The solid lines represent the original ANOPP 1/3-octave *SPL* predictions for the total (black) and combustion (red) noise. The black squares correspond to the total noise signature from the EVNERT experiment, which is reasonably well predicted by the original ANOPP results (see Ref. 23 for details). The dashed curves represent the post-corrected[46] ANOPP 1/3-octave *SPL* predictions for the total (black) and combustion (red) noise using the simplified Pratt & Whitney acoustic turbine-transmission formula (6) rather than the ANOPP-GE one (3b). It is clear from panels (a)–(c) in Fig. 3 that the total noise signature is better predicted by the modified ANOPP results as compared to the original ones.

D. A General Multi-Component Model

In general, there could be several independent combustor-noise sources. The (dimensional) combustor-noise mean-square pressure in each 1/3-octave band can then, in line with Eq. (1a), be written as

$$< p^2 >^{(b)} = \frac{\rho_\infty c_\infty \sum_{k=1}^{N_c} \Pi_k \mathcal{D}_k(\theta, f_b)}{4\pi r_s^2} \tag{7a}$$

for the static-engine-test case, where N_c is the number of independent noise sources and Π_k and $\mathcal{D}_k(\theta, f_b)$ denote the total acoustic power and a combined directivity and spectrum function for the k^{th} source. The overall mean-square pressure is given by

$$< p^2 > = \sum_b < p^2 >^{(b)} = \frac{\rho_\infty c_\infty \sum_{k=1}^{N_c} \Pi_k D_k(\theta)}{4\pi r_s^2} = \frac{\rho_\infty c_\infty \Pi D(\theta)}{4\pi r_s^2}\,, \tag{7b}$$

where $D_k(\theta) = \sum_b \mathcal{D}_k(\theta, f^{(b)})$ is a directivity function for the k^{th} component, $\Pi = \sum_{k=1}^{N_c} \Pi_k$ is the total combustor-noise power, and $D(\theta) = \sum_{k=1}^{N_c} \Pi_k D_k(\theta)/\Pi$ is the overall combustor-noise directivity. Both $D_k(\theta)$ and $D(\theta)$ satisfy the normalization condition (1b).

E. Stone et al. Empirical Model

Stone et al.[30] have developed a combustor-noise model based on an empirical fit of static-test data for four common General-Electric turbofan engines (CF6, CF34, CFM56, and GE90) in current use. The core noise was extracted from the experimental total far-field acoustic signature by a clever and iterative application of a jet-noise model.[47,48] For frequencies below the (lowest) turbine blade-passing frequency, they deduced that the combustor noise could be described by a spectrum comprised of three components corresponding to the low-, mid-, and high-frequency ($\sim$ 1 kHz) peaks observed in the revealed core-noise spectrum. The contribution of each component to the total was then correlated with the engine operational parameters.

Stone et al.[30] presented their results in terms of formulas for the component *OASPL* at the 90^o polar angle

$$OASPL_k(\theta = 90^o) = C_k + 10\left[\alpha_k \log Q - \beta_k \log n_f - \log(4\pi r_s^2)\right]\,, \quad k = 1, 2, 3\,, \tag{8a}$$

where

$$Q = \dot{m}_{core} T_\infty^2 \left(\frac{T_{t,ce} - T_{t,ci}}{T_{t,ci}}\right)^2 \left(\frac{P_{t,ci}}{P_\infty}\right)^2 \tag{8b}$$

is the combustion-noise parameter recommended by Huff et al.,[32] the subscript k indicates combustor noise component, n_f is the number of fuel nozzles, and C_k, α_k, and β_k are constants (Table 1). The $k = 1$ through 3 cases are referred to as the low-, mid-, and high-frequency components, respectively. In regard to the parameter n_f in Eq. (8a), the authors of Ref. 30 state that during their data reduction: *"The fuel nozzle number n_f emerged as a possible correlating parameter, but further analyses might yield better alternative approaches."*

The values of constants α_k and β_k in Table 1 agree with the corresponding ones given in Ref. 30. However, the constants C_k are modified here for two reasons. First, and the major reason, their formula (Ref. 30, Eq. 3) corresponding to Eq. (8a) does not strictly represent the predicted component *OASPL* at the 90^o polar angle. Their quantity *UOL*, somewhat in contradiction to their nomenclature, represents only an intermediate result of the fitting

Table 1. Modified Stone et al.[30] Constants

	$k=1$	$k=2$	$k=3$
C_k	89.69	71.30	53.93
α_k	0.7	1.0	0.9
β_k	1.4	1.8	0.0

procedure and not the final result. To remove this artifact of their fitting procedure, and for clarity, $(0.70, 0.01, 0.44)$ should be added to their values. Second, for consistency with other formulas herein, the factor 4π is explicitly used in the spherical spreading term in Eq. (8a). This means that $10\log(4\pi) \approx 10.99$ should also be added to the constants to obtain the C_k values used herein. Furthermore, note that the constant C_k in Eq. (8a) depends on the units used, i.e., the underlying formulation is not quite dimensionally correct. In addition, as the fitting parameter α_k is changed, the underlying dimension of C_k also changes.[c] The consequence of this is that *in Eqs. (8a,b), the source-to-observer distance must be in ft, the mass flow rate must be in lb_m/s, and the ambient temperature must be in ^oR.* No other equation in this paper has this type of restriction.

The component sound pressure level $SPL^{(b)}$ in each 1/3-octave frequency band and component *OASPL* are given by

$$SPL_k^{(b)} = OASPL_k(\theta{=}90^o) + \mathcal{I}_k(\theta, St_k^{(b)})\,, \quad k = 1,2,3\,, \tag{9a}$$

$$OASPL_k = OASPL_k(\theta{=}90^o) + \Delta OASPL_k(\theta)\,, \quad k = 1,2,3\,, \tag{9b}$$

where $\mathcal{I}_k(\theta, St_k^{(b)})$ is a directivity and frequency index (Tables 2–4),

$$\Delta OASPL_k(\theta) = 10\log\left[\sum_b 10^{\mathcal{I}_k(\theta, St_k^{(b)})/10}\right]\,, \tag{9c}$$

and $St_k^{(b)}$ is a nondimensional frequency (Strouhal number), all for the k^{th} component. The index function $\mathcal{I}_k(\theta, St_k^{(b)})$ in Eq. (9a) is simply the component 1/3-octave *SPL* normalized by the component *OASPL* value in the 90^o polar direction. The Tables 2–4 correspond to the Tables I–III in Ref. 30 adjusted such that $\Delta OASPL_k(\theta{=}90^o) = 0$. The Strouhal number St_k for the three components are given by

$$St_1 = f_b d_{cn}^{(h)}/c_\infty\,, \tag{9d}$$

$$St_k = f_b d_c/c_{ce} \quad k = 2,3\,, \tag{9e}$$

where $d_{cn}^{(h)}$ is the hydraulic diameter of the core nozzle, d_c is the combustor diameter, and c_{ce} is the speed of sound at the combustor exit. The authors of Ref. 30 state: *"The characteristic lengths and velocities used in these Strouhal relations may very well change if data for other engines over a wider range of correlating variables become available. The selection of the currently used characteristic velocities and lengths was based simply on identifying a set that approximately correlated engine-to-engine trends and the fairly small trends with engine power. No claim is made that better relationships cannot be found with further study."*

The fit of the model to the extracted component *OASPL* at 90^o polar angle is reasonably good (Ref. 30, Fig. 12), with only a few data points outside of ± 3 dB error bands. The *SPL*-predictions for the low-, mid-, and high-frequency components (Ref. 30, Figs. 13-15) are also reasonable (again using ± 3 dB as a measure), with the low-frequency and high-frequency component predictions being the best and the least good, respectively. Stone et al.[30] make the following comment on the quality of their fit: *"Since it is impossible to exactly determine the contribution of core noise, statistical accuracy is evaluated on the basis of total noise at frequencies below blade passage. On this basis, the prediction agrees with the data for the four GE engines exactly on average, with root-mean-square error of 1.7 dB."* The fit to the underlying data set is, in fact, remarkably good and is a testament to the well-honed modeling skills of the investigators.

As an initial test of the applicability of the developed model to other turbofan engines, Stone et al.[30] compared predictions to available combustor-noise data, extracted using a three-signal source-separation method[17] from static-engine test data, for a Pratt & Whitney JT15D engine[31] (Ref. 30, Fig. 19) and an Avco Lycoming YF102 engine[17]

[c]This is not uncommon for empirical relationships used in engineering practice and does not limit the potential value for practical application.

(Ref. 30, Fig. 20). For this type of validation testing, it is often difficult to obtain both the required noise and engine-cycle data as well as sufficient engine-geometry information. Stone et al.[30] had to estimate some of the geometric parameters and assume the number of fuel nozzles for both engines—see their report for a discussion of the details and possible impacts on their comparison. For the JT15D-engine and YF102-engine comparisons, the low-frequency combustor-noise component predictions were reduced by 8 dB and 15 dB, respectively, to produce the results shown in their figures. Even with these significant adjustments of the predictions, their results are only in *"rough agreement"* with the experimental data, with differences well exceeding 3 dB for several frequencies. They indicate: *"At present, the reason for the substantial adjustment required for the level of the lowest frequency component is unknown. It will probably be necessary to adjust both the jet and core noise models to improve the accuracy and generality of the model. Differences for the other components may be due to approximations in the combustor parameters, including frequency-scaling effects. Data from more engine geometries and manufacturers would be useful to resolve these issues."* Contrary to their[30] determination, it is concluded here that, at present, their model is *not* capable of predicting the combustion noise associated with the two non-GE engines examined. Thus, for now, the use of the new Stone et al.[30] combustor-noise prediction method should be limited to situations involving only General-Electric turbofan engines.

F. Previous Multi-Component Models

The combustor-noise data for the YF102 and JT15D engines, discussed above, as well as corresponding data for a CF6-50 engine were further examined and correlated by von Glahn and Krejsa.[31] The suggested correlations utilized one, two, and four spectral segments to capture perceived peaks in the far-field combustor-noise spectra. Generally, the sound pressure levels at the single-segment spectrum peak, the higher frequency two-segment spectrum peak, and the two higher frequency four-segment spectrum peaks scaled with a heat-release parameter, as in the semi-empirical models described above, whereas the low-frequency segments scaled with the combustor exit velocity to the fourth power. They stated that the four-segment spectra provided the best overall fit to the data, but also that the two-segment spectrum appeared to be a reasonable representation of the combustion noise. However, their data comparisons do not generally show the expected 3 dB increase at the intersection of the multisegment spectra, which renders their conclusions less clear. Nevertheless, their results show that the assumption of a single-peaked far-field combustion-noise spectrum with the peak fixed at 400 Hz, as used in ANOPP, can be questioned.

Gliebe et al.[49] also developed empirical combustor-noise correlations based on existing static-engine test data for a selection of modern high-bypass-ratio engines. The data used was from General Electric CF6-80C2 and CFM International CFM56-5B/7B engines equipped with single-annular combustors (SAC) and General Electric GE90 and CFM56-5B/7B engines equipped with dual-annular combustors (DAC). They adopted the multi-element spectrum ideas of von Glahn and Kresja[31] and found that the best fits were obtained by using a three-segment spectrum (peaks at 63, 160, and 630 Hz) for SAC engines and two spectral segments (peaks at 160 and 500 Hz) for DAC engines.

III. Combustor Modal Analysis

The essential ingredients in predicting combustor noise are: first, the understanding of the fluctuating pressure and entropy fields, i.e., the source characteristics, inside the combustor and, second, their further propagation and interaction with turbine stages through the turbofan core. Karchmer[24] and Royalty and Schuster[29] have documented the modal structure of the unsteady pressure field in combustors. Karchmer's[24] rig-experiment utilized a ducted full-scale YF102 annular-combustor, whereas Royalty and Schuster[29] analyzed measurements in a real-engine environment. Krejsa and Karchmer[26] have documented the modal structure in the core nozzle of a turbofan engine. The combustor unsteady entropy field and its propagation and interaction with the turbine are still areas of emerging understanding and active research (eg. the propulsion-noise component of the NASA Fundamental Aeronautics Program Quiet Aircraft Subproject).

In the rig experiment, Karchmer[24] analyzed unsteady pressure data obtained from six probes arranged circumferentially in the outer annular wall of the combustor liner at a single axial location for operating conditions roughly corresponding to 30 through 60 percent YF102-engine power. For all conditions, his modal decomposition showed that higher-order azimuthal modes were present in the combustor for frequencies higher than about 400 Hz and that each mode, in sequence, dominated the spectrum near its estimated cut-on frequency (Ref. 24, Fig. 7). That is, successive distinct portions of the pressure spectrum in the combustor could be uniquely identified with a single mode, starting with the plane wave and followed in turn by modes with increasing azimuthal indexes. He concluded that the basic source generating mechanism is relatively smooth and somewhat featureless, but that the annular geometry

of the combustor is extremely effective in modifying the unsteady pressure spectrum in the combustor. Karchmer[24] also carried out limited comparisons with existing far-field results[11] from an YF102 turbofan engine and found rough similarities between his isolated-component results and the full-engine measurements.

Royalty and Schuster[29] analyzed the acoustic modes in the combustor for a particular EVNERT[45] configuration of the TECH977 turbofan engine in which the fan was replaced by a water brake in order to remove fan sources from the total noise signature. The no-fan configuration could be operated up to a power setting corresponding to the approach condition of 60 % corrected fan speed. The combustor internal instrumentation consisted of a circumferential array of 16 equally-spaced pressure probes. They[29] (see their Fig. 19) found that for low frequencies most of the acoustic energy was associated with the plane wave ($m = 0$) mode, that the first circumferential mode ($m = \pm 1$) was dominant in the frequency range of 500–1000 Hz, and that higher circumferential modes ($m = \pm 2$, $m = \pm 3$, $m = \pm 3$, ...) sequentially became the most significant feature at successively higher frequencies, where m is the azimuthal wave number or mode order. One can observe in their figure that at 500 Hz, the plane wave mode is about 8 dB and 5 dB below the total acoustic level at the 48 % and 60 % power settings, respectively. They also reported that the higher modes ($m \neq 0$) were not present in the far-field data. It is concluded here that this indicates that the non-plane-wave modes are cut-off in the turbine/duct downstream of the combustor for this particular engine. This is in agreement with the results of Hultgren and Miles[23] in which coherent combustor noise was only detected for frequencies less than about 400+ Hz.

Krejsa and Karchmer[26] documented the modal structure of the pressure field near the inlet and exit of the core nozzle of an AiResearch Quiet-Clean-General-Aviation-Turbofan (QCGAT) engine for several operating conditions using an array of five circumferentially spaced probes at each axial location. The QCGAT engine was derived from the AiResearch TFE731-3 engine for use in the NASA QCGAT program[50] to demonstrate the applicability of large turbofan engine noise and pollution reduction technology to small general aviation turbofan engines. Their analysis of the pressure data showed that the plane-wave mode was dominant at the very lowest frequencies and that, up to the 1500 Hz upper limit of their analysis, the most recently cut-on azimuthal mode was dominant with increasing frequency. The contribution of modes other than the dominant mode was usually small. At the core tailpipe exit, this meant that the plane wave mode was dominant for frequencies below about 800–900 Hz and that the first azimuthal mode was dominant for higher frequencies.

As pointed out by Schuster and Lieber,[41] these results[24,26] strongly suggest that resonances in the the combustor and tailpipe play an important role in determining the peaks observed in external spectra. They remark that these peaks arise from the modulation of a base spectrum due to the location of the source inside a partially confined geometry consisting of the combustor, turbine, and exhaust nozzle. Further, the far-field spectrum can be thought of as the product of a single peak broadband combustion noise spectrum, that is representative of the spectrum of an open turbulent flame, and a spectral transfer function that is representative of the resonance and propagation effects in the engine core and exhaust. They observe that this transfer function should depend on the duct geometry, gas properties, and impedance conditions at system boundaries, and that "*it is unrealistic to expect that a single transfer relation will be generally applicable to the wide variety of combustor, turbine and exhaust geometries.*" However, through an analysis of narrowband acoustic data from turbofans, turboshafts, and auxiliary power units (APUs) manufactured by Honeywell, they found that the far-field combustor-noise peak frequencies correlated strongly with the exhaust duct length and mean exhaust duct sound speed according to plane-wave radiation from an unflanged circular pipe. This led to the development and ultimate implementation of the intermediate-narrow-band model, briefly discussed in § IIB, into ANOPP.

IV. Results

The three-spectrum model proposed by Stone et al.[30] for GE turbofan-engine combustor noise is compared with ANOPP-formula predictions for several relevant cases. The computations are carried out using MATLAB scripts implementing Eqs. (1)–(3) and (6) for the ANOPP models and Eqs. (8) and (9) for the Stone et al. model. The static-engine-test results are presented for a free-space virtual observer at a one-foot distance and are lossless, i.e. atmospheric attenuation is not included in the predictions. The engine operational parameters are taken to correspond to Rolling-Takeoff (RTO) power at Sea-Level-Standard 25 ^{o}C (SLS+10K) conditions (warm day).

A. GE90-94B Predictions

Figure 4 shows the 1/3-octave *SPL* spectra in the 90, 120, and 150 degree directions and the *OASPL* versus polar angle for the takeoff condition (RTO-SLS+10K). The engine operational point corresponds to the related far-field results presented in Figs. 10(c)–(e) and 11 of Ref. 30. The figure shows the contributions from the low-, mid-, and high-frequency components as well as the total from the Stone et al. model, and the prediction using the SAE method with the GE turbine-attenuation factor (SAE-GE).

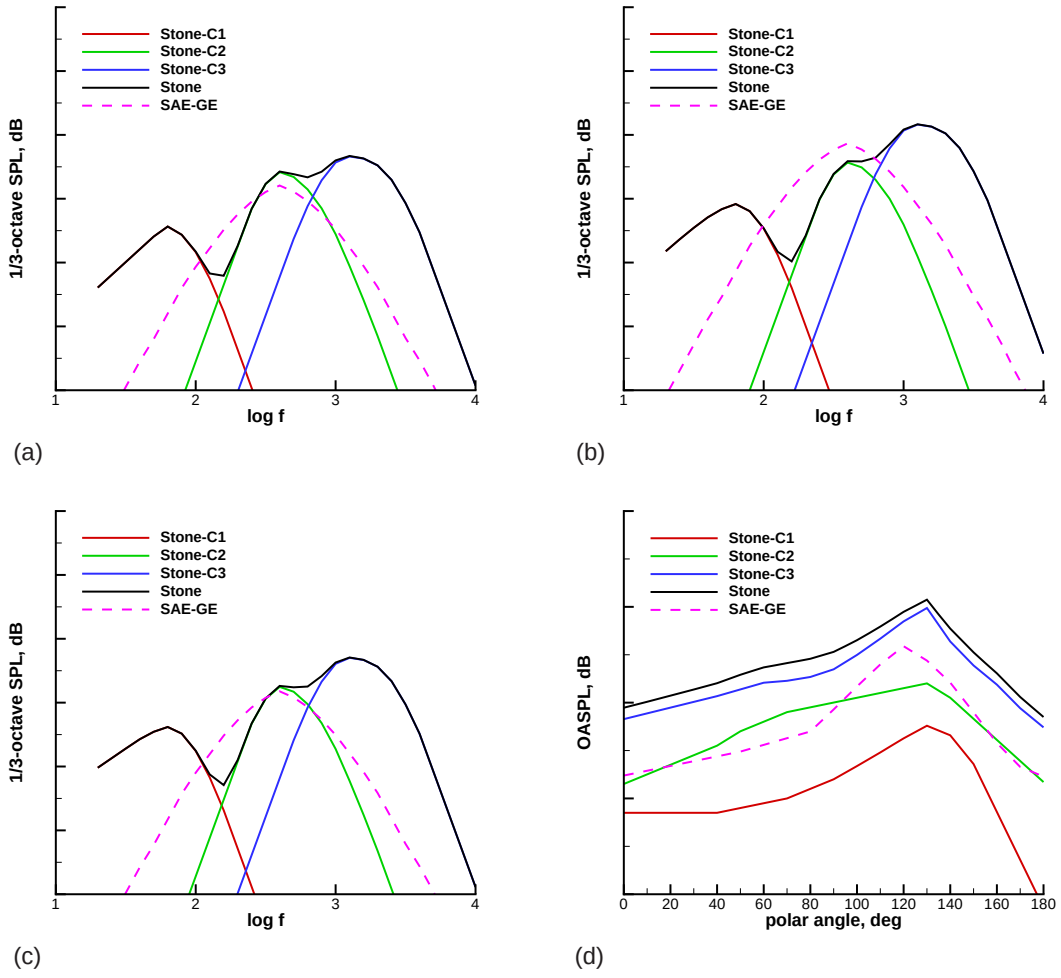

Figure 4. Comparison of one-foot loss-less combustor-noise predictions using the Stone et al.[30] and ANOPP SAE-GE formulas for a GE90-94B turbofan engine at Rolling Takeoff power and Sea-Level-Standard 25 ^{o}C conditions; red, green, and blue lines—Stone method low-, mid-, and high-frequency contributions; black lines—Stone method; dashed magenta lines—SAE-GE method; major tick marks on vertical axis represent 10 dB increments; (a)–(c): 1/3-octave SPL versus 1/3-octave center frequency in the 90^{o}, 120^{o}, and 150^{o}, directions; (d): OASPL versus polar angle

A visual overview of the difference between the predictions is shown in Fig. 5 where side-by-side carpet plots of

the 1/3-octave SPL as function of frequency and polar angle are shown also for the takeoff condition. The left panel in the figure shows the total Stone et. al. model result and the right panel shows the SAE-GE result.

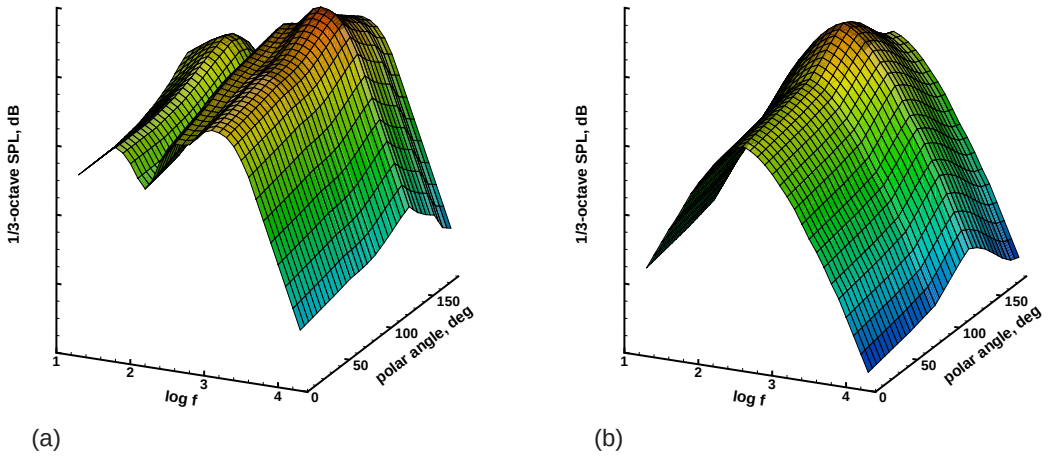

Figure 5. Predicted one-foot loss-less combustor-noise 1/3-octave SPL as function of 1/3-octave center frequency and polar angle for a GE90-94B turbofan engine at Rolling Takeoff power and Sea-Level-Standard 25 ^{o}C conditions; major tick marks on vertical axis represent 20 dB increments; (a): Stone et al.[30] method; (b): ANOPP SAE-GE method

As can be seen in Figs. 4 and 5, essentially the SAE spectral distribution is replaced by the more narrow mid-frequency component distribution, with basically the same spectral-peak frequency, as well as with low- and high-frequency components. The peak levels of the SAE prediction and the mid-level Stone et al. component are comparable, with a difference of less than about 3 dB, which is also reflected in their $OASPL$ distributions shown in Fig. 4(d). Because the high-frequency component has, clearly, a higher level than the other two components in the aft quadrant, the total Stone et al. $OASPL$ levels are higher compared to the SAE-GE prediction, with the peak being about 5 dB higher. The total Stone et al. $OASPL$ peak also occurs at a 10^{o} more shallow angle with respect to the downstream direction than the corresponding SAE-GE peak.

B. Energy Efficient Engine Predictions

The Energy Efficient Engine (E^3) Program[51–53] (late 1970s to mid 1980s) was a NASA funded effort to develop technologies that would significantly reduce fuel consumption and operating costs of (then) future transport aircraft engines. Both Pratt & Whitney and General Electric were major participants in this highly successful project. Both companies initially conducted separate flight-propulsion-system design and analysis studies (see Ref. 51 for references), but because of budget constraints only General Electric was selected to build a technology-demonstration engine,[54] for integrated core/low-spool testing, whereas the Pratt & Whitney effort was limited to component-technology testing. The technologies developed during this program have been effectively adopted by the engine manufacturers. In particular, the General Electric demonstrator engine, commonly referred to as the E^3 engine, formed the kernel of what eventually became their GE90 turbofan. Because the E^3 engine can be thought of as part of the GE-turbofan family, but was not part of the data fit in Ref. 30, it is a suitable candidate for the comparisons carried out here. In addition, there are non-proprietary mean-flow properties available,[d] obtained through use of the Numerical Propulsion System Simulation[55] (NPSS) computer program, for the E^3 engine.

Figure 6 shows the 1/3-octave SPL spectra in the 90, 120, and 150 degree directions and the $OASPL$ versus polar angle for the takeoff condition (RTO-SLS+10K). The figure shows the contributions from the low-, mid-, and high-frequency components as well as the total from the Stone et al. model, and the prediction using the SAE method with the GE turbine-attenuation factor (SAE-GE). As can be seen in Fig. 6, the spectral-peak frequencies for the SAE distribution and the more narrow mid-frequency component distribution are essentially the same, but their spectral peak levels are not as close as in Fig. 4. The $OASPL$ levels of the SAE-GE method and the total Stone et al. prediction are comparable in the aft quadrant. However, the latter has a slightly higher peak at a shallower polar angle due to

[d] Claus, R. W., Private Communication

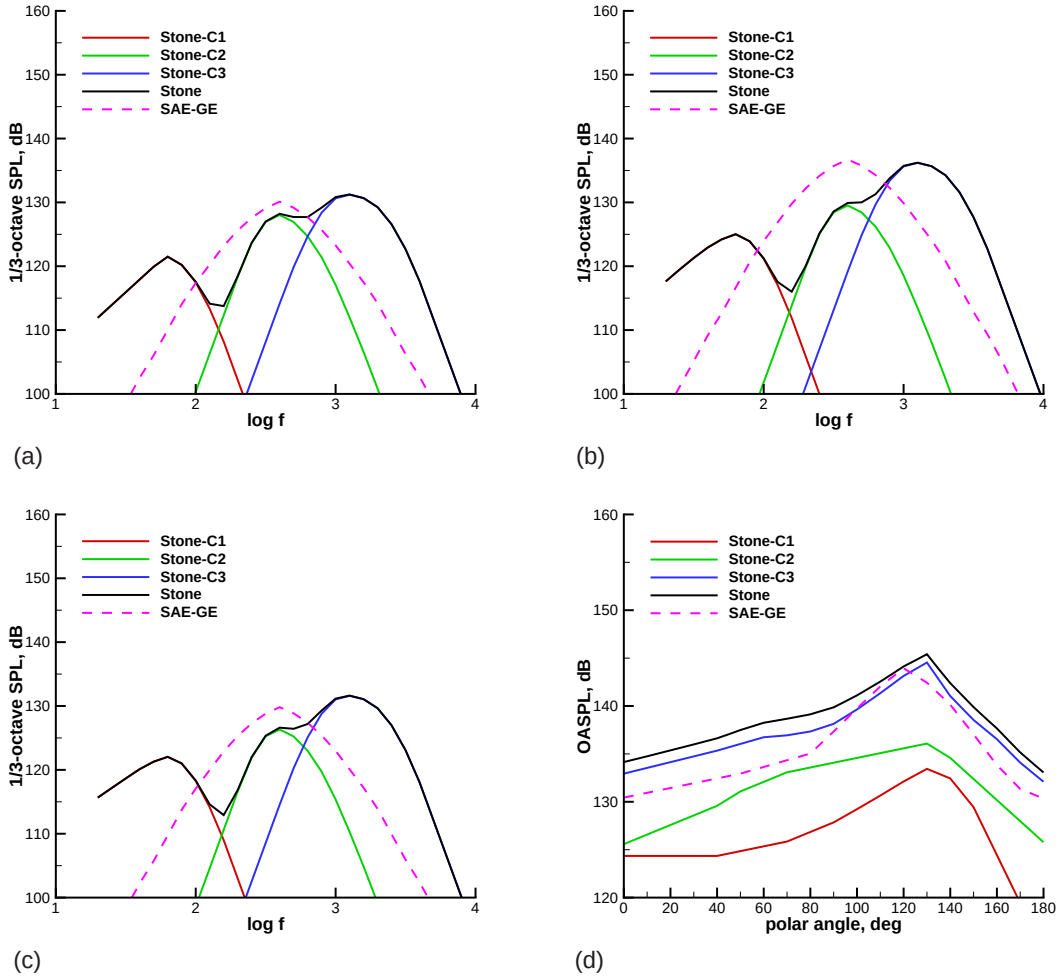

Figure 6. Comparison of one-foot loss-less combustor-noise predictions using the Stone et al.[30] and ANOPP SAE-GE formulas for an E^3 turbofan engine at Rolling Takeoff power and Sea-Level-Standard 25 ^{o}C conditions; red, green, and blue lines—Stone method low-, mid-, and high-frequency contributions; black lines—Stone method; magenta lines—SAE-GE method; major tick marks on vertical axis represent 10 dB increments; (a)–(c): 1/3-octave SPL versus 1/3-octave center frequency in the 90^o, 120^o, and 150^o, directions; (d): OASPL versus polar angle

contributions from the high-frequency component. The difference in the predicted *OASPL* levels in the 110^o to 140^o polar angle range, which from a practical point of view is the important direction, is less than about 3 dB.

C. TECH977 Predictions

Figure 7 shows the 1/3-octave *SPL* spectra in the 90, 120, and 150 degree directions and the *OASPL* versus polar angle for the takeoff condition (RTO-SLS+10K). The figure shows the contributions from the low-, mid-, and high-frequency components as well as the total from the Stone et al. model, and the prediction using the SmE method with the PW turbine-attenuation factor (SmE-PW). Here, the SmE-PW spectral distribution is essentially mimicked by the low-frequency component in the Stone et al. method. The peak levels are within about 6 dB of each other in the 120^o direction, but the peak of the low-frequency component occurs at one 1/3-octave frequency band lower than SmE-PW peak does. Their *OASPL* distributions are also quite similar, with values within 3 dB of each other, but the SmE-PW peak occurs at a 10^o less shallow angle (120^o versus 130^o) with respect to the downstream direction. The total Stone et al. *OASPL* peak is also about 4 dB higher than the SmE-PW one. Figure 7 also shows that the spectral peaks of the mid- and high-frequency components in the Stone et al. method predictions fall above 1 kHz, with levels at least comparable to that of the low-frequency component. The implication from the Stone et al. method prediction shown in this figure, i.e., that there would be a significant amount of combustor noise present for frequencies higher than

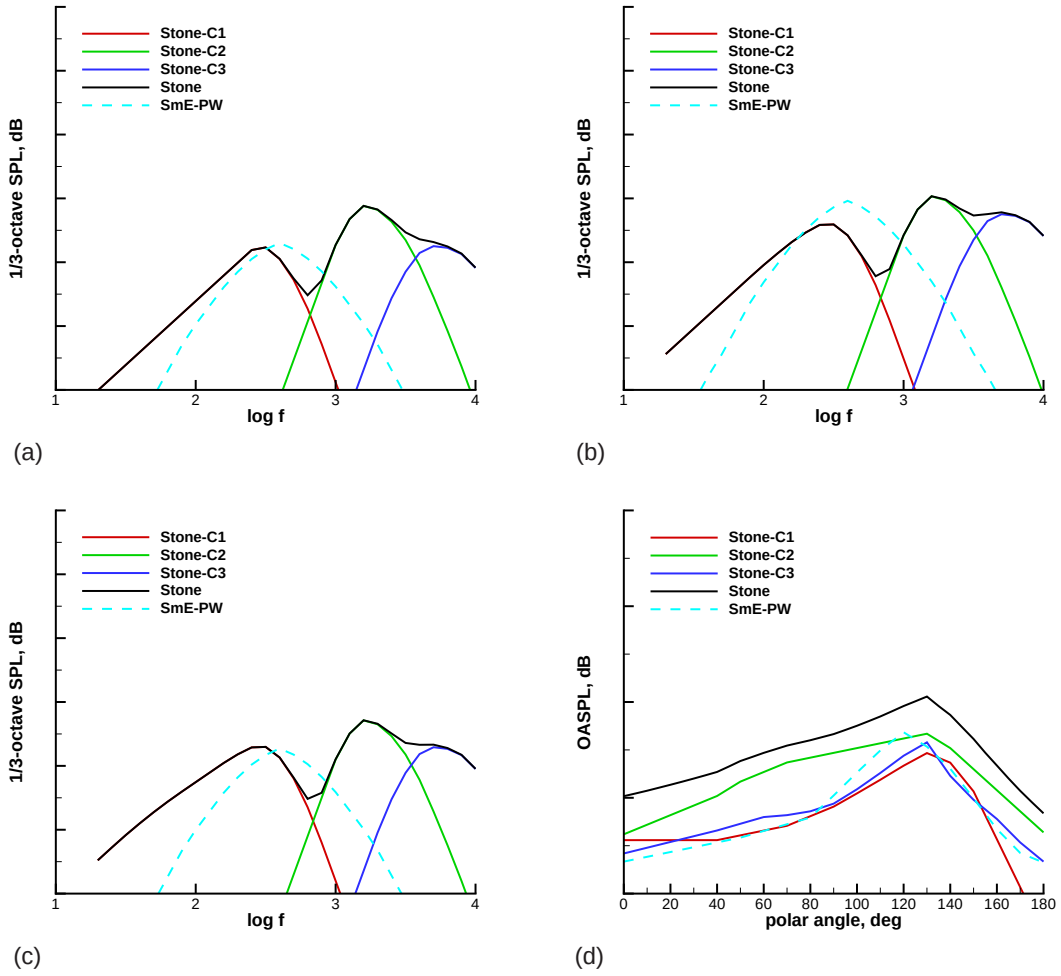

Figure 7. Comparison of one-foot loss-less combustor-noise predictions using the Stone et al.[30] and ANOPP SmE-PW formulas for a TECH977 turbofan engine at Rolling Takeoff power and Sea-Level-Standard 25 ^{o}C conditions; red, green, and blue lines—Stone method low-, mid-, and high-frequency contributions; black lines—Stone method; dashed cyan lines—SmE-PW method; major tick marks on vertical axis represent 10 dB increments; (a)–(c): 1/3-octave SPL versus 1/3-octave center frequency in the 90^{o}, 120^{o}, and 150^{o}, directions; (d): OASPL versus polar angle

1 kHz, is in direct contradiction with prior analyses[22,23,29,46] of EVNERT TECH977 acoustic data. Even though there are some uncertainties in the actual values used for the geometry parameters in Eqs. (9d) and (9e), to determine the component Strouhal numbers, these are not large enough to invalidate the conclusion that the Stone et al.[30] method is not suitable for combustor-noise predictions for the Honeywell TECH977 research turbofan.

V. Summary and Conclusions

A brief history of semi-empirical combustor noise modeling has been given. The current status of combustor-noise prediction in NASA ANOPP has been described and near-term improvements have been discussed. The alternate turbine-transmission factor, described in §IIC, will appear as a user selectable option in the combustor-noise module GECOR in the next release of ANOPP and the Stone et al.[30] method is scheduled to be implemented as a separate ANOPP module later this year.[e] Based on the discussion and results presented herein, it is recommended that *the application of the new empirical Stone et al.[30] combustor-noise prediction method be limited to situations involving only General-Electric turbofan engines.*

Further progress on an intermediate time frame is probably best achieved by following the research direction

[e]Burley, C. L., Private Communication

of Schuster and Lieber,[41] based partly on insights in Karchmer's[24] work, namely to develop better engine-transfer functions for combustion noise rather than pursuing empirical multi-peak modeling activities that have less direct connection to the underlying physics.

Because the impact of other propulsion-noise sources continues to be reduced due to turbofan design trends, advances in noise-mitigation techniques, and expected aircraft configuration changes, the relative importance of core noise is expected to greatly increase in the future. Combustor noise, an important core-noise component, needs to be studied and mitigated in order to meet future noise goals. The noise-source structure in the combustor, including the indirect one, and the effects of the propagation path through the engine and exhaust nozzle need to be better understood. In particular, the acoustic consequences of the expected trends toward smaller, highly efficient gas-generator cores and low-emission fuel-flexible combustors need to be fully investigated since future designs are quite likely to be outside of the parameter space of existing (semi-empirical) prediction tools. This will require a concerted research effort involving rig-testing at near-engine conditions, full-engine testing, high-fidelity simulations, as well as reduced-order and multi-fidelity modeling activities. This will enable the required further development of propulsion-noise prediction methods and core-noise mitigation technologies.

References

[1] Berton, J. B., Envia, E., and Burley, C. L., "An Analytical Assessment of NASA's N+1 Subsonic Fixed Wing Project Noise Goal," Tech. Rep. AIAA Paper 2009-3144, 16th AIAA/CEAS Aerocoustics Conference, Miami, Florida, 2009.

[2] Cumpsty, N. A. and Marble, F. E., "The Interaction of Entropy Fluctuations with Turbine Blade Rows; a Mechanism of Turbojet Engine Noise," *Proc. R. Soc. Lond. A*, Vol. 357, 1977, pp. 323–344.

[3] Cumpsty, N. A. and Marble, F. E., "Core Noise from Gas Turbine Exhausts," *J. Sound and Vibration*, Vol. 54, No. 2, 1977, pp. 297–309.

[4] Cumpsty, N. A., "Jet Engine Combustion Noise: Pressure, Entropy and Vorticity Perturbations Produced by Unsteady Combustion or Heat Addition," *J. Sound and Vibration*, Vol. 66, No. 4, 1979, pp. 527–544.

[5] Mathews, D. C., Rekos, Jr, N. F., and Nagel, R. T., "Combustion Noise Investigation," Tech. Rep. FAA RD-77-3, FAA, 1977.

[6] Miles, J. H., "Spectral Separation of the Turbofan Engine Coherent Combustion Noise Component," Tech. Rep. AIAA Paper 2008-0050 (NASA TM-2008-215157), 46th Aerospace Sciences Meeting, Reno, Nevada, 2008.

[7] Miles, J. H., "Time Delay Analysis of Turbofan Engine Direct and Indirect Combustion Noise Sources," *J. Propulsion and Power*, Vol. 25, No. 1, 2009, pp. 218–227.

[8] Mahan, R. J. and Karchmer, A., "Combustion and Core Noise," *Aeroacoustics of Flight Vehicles: Theory and Practice*, edited by H. H. Hubbard, Vol. 1, chap. 9, NASA Reference Publication 1258, WRDC Technical Report 90-3052, 1991, pp. 483–517.

[9] Bendat, J. S. and Piersol, A. G., *Engineering Applications of Correlation and Spectral Analysis*, Wiley-Interscience, 1980.

[10] Karchmer, A. M. and Reshotko, M., "Core Noise Source Diagnostics on a Turbofan Engine Using Correlation and Coherence Techniques," Tech. Rep. NASA TM-X-73535, NASA, 1976.

[11] Reshotko, M., Karchmer, A. M., Penko, P. F., and McArdle, J. G., "Core Noise Measurements on a YF-102 Turbofan Engine," *J. Aircraft*, Vol. 14, No. 7, 1977, pp. 611–612.

[12] Karchmer, A. M., "Identification and Measurement of Combustion Noise from a Turbofan Engine Using Correlation and Coherence Techniques," Tech. Rep. NASA TM-73747, NASA, 1977.

[13] Karchmer, A. M., Reshotko, M., and Montegani, F. J., "Measurement of Far-Field Combustion Noise from a Turbofan Engine Using Coherence Functions," Tech. Rep. AIAA Paper 1977-1277 (NASA TM-73748), 4th AIAA Aeroacoustics Conference, Atlanta, Georgia, 1977.

[14] Chung, J. Y., "Rejection of Flow Noise Using a Coherence Function Method," *J. Acoustical Society of America*, Vol. 62, No. 2, 1977, pp. 388–395.

[15] Reshotko, M. and Karchmer, A. M., "Core Noise Measurements from a Small, General Aviation Turbofan Engine," Tech. Rep. NASA TM-81610, NASA, 1980.

[16] Doyle, V. L. and Moore, M. T., "Core Noise Investigation of the CF6-50 Turbofan Engine," Tech. Rep. NASA CR-159749, NASA, 1980.

[17] Krejsa, E. A., "New Technique for the Direct Measurement of Core Noise from Aircraft Engines," Tech. Rep. AIAA Paper 1981-1587 (NASA TM-82634), 17th AIAA/SAE/ASME Joint Propulsion Conference, Colorado Springs, Colorado, 1981.

[18] Krejsa, E. A., "Application of 3-Signal Coherence to Core Noise Transmission," Tech. Rep. AIAA Paper 1983-0759 (NASA TM-83333), 8th AIAA Aeroacoustics Conference, Atlanta, Georgia, 1983.

[19] Shivashankara, B. N., "High Bypass Ratio Engine Noise Component Separation by Coherence Technique," *J. Aircraft*, Vol. 20, No. 3, 1983, pp. 236–242.

[20] Krejsa, E. A., "Combustion Noise From Gas Turbine Aircraft Engines Measurement of Far-Field Levels," Tech. Rep. NASA TM-88971, NASA, 1987.

[21] Hsu, J. S. and Ahuja, K. K., "A Coherence-Based Technique to Separate Internal Mixing Noise From Farfield Measurements," Tech. Rep. AIAA Paper 1998-2296, 4th AIAA/CEAS Aeroacoustic Conference, Toulouse, France, 1998.

[22] Mendoza, J. M., Nance, D. K., and Ahuja, K. K., "Source Separation from Multiple Microphone Measurements in the Far Field of a Full Scale Aero Engine," Tech. Rep. AIAA Paper 2008-2809, 14th AIAA/CEAS Aeroacoustic Conference, Vancouver, British Columbia, 2008.

[23] Hultgren, L. S. and Miles, J. H., "Noise-Source Separation Using Internal and Far-Field Sensors for a Full-Scale Turbofan Engine," Tech. Rep. AIAA Paper 2009-3220 (NASA TM-2009-215834), 15th AIAA/CEAS Aeroacoustic Conference, Miami, Florida, 2009.

[24] Karchmer, A. M., "Acoustic Modal Analysis of a Full Scale Annular Combustor," Tech. Rep. AIAA Paper 1983-0760 (NASA TM-83334), 8th AIAA Aeroacoustics Conference, Atlanta, Georgia, 1983.

[25]Miles, J. H. and Krejsa, E. A., "Pressure Transfer Function of a JT15D Nozzle due to Acoustic and Convected Entropy Fluctuations," *J. Acoustical Society of America*, Vol. 72, No. 6, 1982, pp. 2008–2019.

[26]Krejsa, E. A. and Karchmer, A. M., "Acoustic Modal Analysis of the Pressure Field in the Tailpipe of a Turbofan Engine," Tech. Rep. NASA TM-83387, NASA, 1983.

[27]Miles, J. H., Wasserbauer, C. A., and Krejsa, E. A., "Cross Spectra Between Temperature and Pressure in a Constant Area Duct Downstream of a Combustor," Tech. Rep. AIAA Paper 1983-0762 (NASA TM-83351), 8th AIAA Aeroacoustics Conference, Atlanta, Georgia, 1983.

[28]Miles, J. H., Wasserbauer, C. A., and Krejsa, E. A., "Cross Spectra Between Pressure and Temperature in a Constant-Area Duct Downstream of a Hydrogen-Fueled Combustor," Tech. Rep. NASA TM-83463, NASA, 1983.

[29]Royalty, C. M. and Schuster, B., "Noise from a Turbofan Engine Without a Fan from the Engine Validation of Noise and Emission Reduction Technology (EVNERT) Program," Tech. Rep. AIAA 2008-2810, 14th AIAA/CEAS Aeroacoustics Conference, Vancouver, British Columbia, 2008.

[30]Stone, J. R., Krejsa, E. A., and Clark, J. C., "Enhanced Core Noise Modeling for Turbofan Engines," Tech. Rep. NASA CR-2011-217026, NASA, 2011.

[31]von Glahn, U. and Krejsa, E. A., "Correlation of Core Noise Obtained by Three-Signal Coherence Techniques," Tech. Rep. NASA TM-83012, NASA, 1982.

[32]Huff, R. G., Clark, B. J., and Dorsch, R. G., "Interim Prediction Method for Low Frequency Core Engine Noise," Tech. Rep. NASA TM X-71627, NASA, 1974.

[33]Zorumski, W. E., "Aircraft Noise Prediction Program Theoretical Manual, Part 1," Tech. Rep. NASA TM-83199-Pt-1, NASA, 1982.

[34]Zorumski, W. E., "Aircraft Noise Prediction Program Theoretical Manual, Part 2," Tech. Rep. NASA TM-83199-Pt-2, NASA, 1982.

[35]Motsinger, R., "Prediction of Engine Combustor Noise and Correlation with T64 Engine Low Frequency Noise," Tech. Rep. R72AEG313, General Electric Co., 1972.

[36]Dunn, D. G. and Peart, N. A., "Aircraft Noise Source and Contour Estimation," Tech. Rep. NASA CR-114649, NASA, 1973.

[37]Society of Automotive Engineers International, "Gas Turbine Jet Exhaust Prediction," Tech. Rep. SAE ARP876 Rev. E, 2006.

[38]Emmerling, J. J., Kazin, S. B., and Matta, R. K., "Core Engine Noise Control Program, Volume III, Supplement 1—Prediction Methods," Tech. Rep. FAA RD-74-125 III-I, FAA, 1976.

[39]Ho, P. Y. and Doyle, V. L., "Combustion Noise Prediction Update," Tech. Rep. AIAA Paper 1979-0588, 5th AIAA Aerocoustics Conference, Seattle, Washington, 1979.

[40]Hough, J. W. and Weir, D. S., "Small Engine Technology (SET)—Task 13 ANOPP Noise Prediction for Small Engines: Jet, Core, and Turbine Module Revisions," Tech. Rep. No. 21-9655, AlliedSignal Engines, Phoenix, Arizona, 1997.

[41]Schuster, B. and Lieber, L., "Narrowband Model for Gas Turbine Engine Combustion Noise Prediction," Tech. Rep. AIAA Paper 2006-2677, 12th AIAA/CEAS Aerocoustics Conference, Cambridge, Massachusetts, 2006.

[42]Mathews, D. C. and Rekos, Jr, N. F., "Prediction and Measurement of Direct Combustion Noise in Turbopropulsion Systems," *J. Aircraft*, Vol. 14, No. 9, 1977, pp. 850–859.

[43]Pickett, G. F., "Core Engine Noise Due to Temperature Fluctuations Convecting Through Turbine Blade Rows," Tech. Rep. AIAA Paper 1975-0528, 2nd AIAA Aero-Acoustics Conference, Hampton, Virginia, 1975.

[44]Zuckerman, R. S., "Core Engine Noise Reduction: Definition and Trends," Tech. Rep. AIAA Paper 1977-1273, 4th AIAA Aeroacoustics Conference, Atlanta, Georgia, 1977.

[45]Weir, D. S., "Engine Validation of Noise and Emission Reduction Technology Phase I," Tech. Rep. NASA CR-2008-215225, NASA, 2008, Honeywell Report No. 21-13843, Honeywell Aerospace, Phoenix, Arizona.

[46]Hultgren, L. S., "Full-Scale Turbofan-Engine Turbine-Transfer Function Determination Using Three Internal Sensors," Tech. Rep. AIAA Paper 2011-2912 (NASA TM-2012-217252), 17th AIAA/CEAS Aeroacoustic Conference, Portland, Oregon, 2011.

[47]Stone, J. R., Krejsa, E. A., and Clark, B. J., "Semi-Empirical Model for Coannular Nozzle Component Noise Extraction and Correlation Including the Effects of Noise Reduction Devices," Tech. Rep. AIAA Paper 2003-1060, 41st AIAA Aeroaspace Sciences Meeting, Reno, Nevada, 2003.

[48]Stone, J. R., Krejsa, E. A., Clark, B. J., and Berton, J. J., "Jet Noise Modeling for Suppressed and Unsuppressed Aircraft in Simulated Flight," Tech. Rep. TM 2009-215524, NASA, 2009.

[49]Gliebe, P., Mani, R., Shin, H., Mitchel, B., Ashford, G., Salamah, S., and Connell, S., "Aeroacoustic Prediction Codes," Tech. Rep. NASA CR-2000-210244, NASA, 2000.

[50]Heldenbrand, R. W. and Norgren, W. M., "Airesearch QCGAT Program," Tech. Rep. NASA CR-159758, NASA, 1979.

[51]Ciepluch, C. C., Davis, D. Y., and Gray, D. E., "Results of NASA's Energy Efficient Engine Program," *J. Propulsion*, Vol. 3, No. 6, 1987, pp. 560–568.

[52]Ethell, J. L., "Fuel Economy in Aviation," Tech. Rep. NASA SP-462, NASA, 1983.

[53]Batterton, P. G., "Energy Efficient Engine Program Contributions to Aircraft Fuel Conservation," Tech. Rep. NASA TM-83741, NASA, 1984.

[54]Davis, D. Y., "Energy Efficient Engine Flight Propulsion System Final Design and Analysis," Tech. Rep. NASA CR-168219, NASA, 1985.

[55]Claus, R. W., Evans, A. L., Lytle, J. K., and Nichols, L. D., "Numerical Propulsion System Simulation," *Computer Systems in Engineering*, Vol. 2, No. 4, 1991, pp. 357–364.

Table 2. Modified Stone et al[30] Low-Frequency Combustor-Noise Component (k=1) Distribution Index

$\log St_1$	$\theta = 0.0$	10.0	20.0	30.0	40.0	50.0	60.0	70.0	80.0	90.0
-3.60	-59.70	-59.70	-59.70	-59.70	-59.70	-59.20	-58.70	-58.20	-57.20	-56.20
-3.50	-57.70	-57.70	-57.70	-57.70	-57.70	-57.20	-56.70	-56.20	-55.20	-54.20
-3.40	-55.70	-55.70	-55.70	-55.70	-55.70	-55.20	-54.70	-54.20	-53.20	-52.20
-3.30	-53.70	-53.70	-53.70	-53.70	-53.70	-53.20	-52.70	-52.20	-51.20	-50.20
-3.20	-51.70	-51.70	-51.70	-51.70	-51.70	-51.20	-50.70	-50.20	-49.20	-48.20
-3.10	-49.70	-49.70	-49.70	-49.70	-49.70	-49.20	-48.70	-48.20	-47.20	-46.20
-3.00	-47.70	-47.70	-47.70	-47.70	-47.70	-47.20	-46.70	-46.20	-45.20	-44.20
-2.90	-45.70	-45.70	-45.70	-45.70	-45.70	-45.20	-44.70	-44.20	-43.20	-42.20
-2.80	-43.70	-43.70	-43.70	-43.70	-43.70	-43.20	-42.70	-42.20	-41.20	-40.20
-2.70	-41.70	-41.70	-41.70	-41.70	-41.70	-41.20	-40.70	-40.20	-39.20	-38.20
-2.60	-39.70	-39.70	-39.70	-39.70	-39.70	-39.20	-38.70	-38.20	-37.20	-36.20
-2.50	-37.70	-37.70	-37.70	-37.70	-37.70	-37.20	-36.70	-36.20	-35.20	-34.20
-2.40	-35.70	-35.70	-35.70	-35.70	-35.70	-35.20	-34.70	-34.20	-33.20	-32.20
-2.30	-33.70	-33.70	-33.70	-33.70	-33.70	-33.20	-32.70	-32.20	-31.20	-30.20
-2.20	-31.70	-31.70	-31.70	-31.70	-31.70	-31.20	-30.70	-30.20	-29.20	-28.20
-2.10	-29.70	-29.70	-29.70	-29.70	-29.70	-29.20	-28.70	-28.20	-27.20	-26.20
-2.00	-27.70	-27.70	-27.70	-27.70	-27.70	-27.20	-26.70	-26.20	-25.20	-24.20
-1.90	-25.70	-25.70	-25.70	-25.70	-25.70	-25.20	-24.70	-24.20	-23.20	-22.20
-1.80	-23.70	-23.70	-23.70	-23.70	-23.70	-23.20	-22.70	-22.20	-21.20	-20.20
-1.70	-21.70	-21.70	-21.70	-21.70	-21.70	-21.20	-20.70	-20.20	-19.20	-18.20
-1.60	-19.70	-19.70	-19.70	-19.70	-19.70	-19.20	-18.70	-18.20	-17.20	-16.20
-1.50	-17.70	-17.70	-17.70	-17.70	-17.70	-17.20	-16.70	-16.20	-15.20	-14.20
-1.40	-15.70	-15.70	-15.70	-15.70	-15.70	-15.20	-14.70	-14.20	-13.20	-12.20
-1.30	-13.70	-13.70	-13.70	-13.70	-13.70	-13.20	-12.70	-12.20	-11.20	-10.20
-1.20	-11.70	-11.70	-11.70	-11.70	-11.70	-11.20	-10.70	-10.20	-9.20	-8.20
-1.10	-9.70	-9.70	-9.70	-9.70	-9.70	-9.20	-8.70	-8.20	-7.20	-6.20
-1.00	-10.80	-10.80	-10.80	-10.80	-10.80	-10.30	-9.80	-9.30	-8.30	-7.30
-0.90	-13.30	-13.30	-13.30	-13.30	-13.30	-12.80	-12.30	-11.80	-10.80	-9.80
-0.80	-17.30	-17.30	-17.30	-17.30	-17.30	-16.80	-16.30	-15.80	-14.80	-13.80
-0.70	-22.30	-22.30	-22.30	-22.30	-22.30	-21.80	-21.30	-20.80	-19.80	-18.80
-0.60	-28.30	-28.30	-28.30	-28.30	-28.30	-27.80	-27.30	-26.80	-25.80	-24.80
-0.50	-34.30	-34.30	-34.30	-34.30	-34.30	-33.80	-33.30	-32.80	-31.80	-30.80
-0.40	-40.30	-40.30	-40.30	-40.30	-40.30	-39.80	-39.30	-38.80	-37.80	-36.80
-0.30	-46.30	-46.30	-46.30	-46.30	-46.30	-45.80	-45.30	-44.80	-43.80	-42.80
-0.20	-52.30	-52.30	-52.30	-52.30	-52.30	-51.80	-51.30	-50.80	-49.80	-48.80
-0.10	-58.30	-58.30	-58.30	-58.30	-58.30	-57.80	-57.30	-56.80	-55.80	-54.80
0.00	-64.30	-64.30	-64.30	-64.30	-64.30	-63.80	-63.30	-62.80	-61.80	-60.80

Table 2. Modified Stone et al[30] Low-Frequency Combustor-Noise Component (k=1) Distribution Index, continued (1)

$\log St_1$	$\theta = 90.0$	100.0	110.0	120.0	130.0	140.0	150.0	160.0	170.0	180.0
-3.60	-56.20	-54.70	-53.00	-50.50	-46.90	-47.90	-50.90	-55.90	-60.90	-65.90
-3.50	-54.20	-52.70	-51.00	-48.50	-44.90	-45.90	-48.90	-53.90	-58.90	-63.90
-3.40	-52.20	-50.70	-49.00	-46.50	-42.90	-43.90	-46.90	-51.90	-56.90	-61.90
-3.30	-50.20	-48.70	-47.00	-44.50	-40.90	-41.90	-44.90	-49.90	-54.90	-59.90
-3.20	-48.20	-46.70	-45.00	-42.50	-38.90	-39.90	-42.90	-47.90	-52.90	-57.90
-3.10	-46.20	-44.70	-43.00	-40.50	-36.90	-37.90	-40.90	-45.90	-50.90	-55.90
-3.00	-44.20	-42.70	-41.00	-38.50	-34.90	-35.90	-38.90	-43.90	-48.90	-53.90
-2.90	-42.20	-40.70	-39.00	-36.50	-32.90	-33.90	-36.90	-41.90	-46.90	-51.90
-2.80	-40.20	-38.70	-37.00	-34.50	-30.90	-31.90	-34.90	-39.90	-44.90	-49.90
-2.70	-38.20	-36.70	-35.00	-32.50	-28.90	-29.90	-32.90	-37.90	-42.90	-47.90
-2.60	-36.20	-34.70	-33.00	-30.50	-26.90	-27.90	-30.90	-35.90	-40.90	-45.90
-2.50	-34.20	-32.70	-31.00	-28.50	-24.90	-25.90	-28.90	-33.90	-38.90	-43.90
-2.40	-32.20	-30.70	-29.00	-26.50	-22.90	-23.90	-26.90	-31.90	-36.90	-41.90
-2.30	-30.20	-28.70	-27.00	-24.50	-20.90	-21.90	-24.90	-29.90	-34.90	-39.90
-2.20	-28.20	-26.70	-25.00	-22.50	-18.90	-19.90	-22.90	-27.90	-32.90	-37.90
-2.10	-26.20	-24.70	-23.00	-20.50	-16.90	-17.90	-20.90	-25.90	-30.90	-35.90
-2.00	-24.20	-22.70	-21.00	-18.50	-15.00	-16.00	-19.00	-24.00	-29.00	-34.00
-1.90	-22.20	-20.70	-19.00	-16.50	-13.20	-14.20	-17.20	-22.20	-27.20	-32.20
-1.80	-20.20	-18.70	-17.00	-14.50	-11.50	-12.50	-15.50	-20.50	-25.50	-30.50
-1.70	-18.20	-16.70	-15.00	-12.50	-9.90	-10.90	-13.90	-18.90	-23.90	-28.90
-1.60	-16.20	-14.70	-13.00	-10.50	-8.40	-9.40	-12.40	-17.40	-22.40	-27.40
-1.50	-14.20	-12.70	-11.00	-8.60	-6.90	-7.90	-10.90	-15.90	-20.90	-25.90
-1.40	-12.20	-10.70	-9.00	-6.80	-5.40	-6.40	-9.40	-14.40	-19.40	-24.40
-1.30	-10.20	-8.70	-7.00	-5.10	-3.90	-4.90	-7.90	-12.90	-17.90	-22.90
-1.20	-8.20	-6.70	-5.20	-3.80	-2.70	-3.70	-6.70	-11.70	-16.70	-21.70
-1.10	-6.20	-4.90	-3.70	-2.70	-1.70	-2.70	-5.70	-10.70	-15.70	-20.70
-1.00	-7.30	-6.00	-4.70	-3.60	-2.50	-3.50	-6.50	-11.50	-16.50	-21.50
-0.90	-9.80	-8.50	-7.20	-6.10	-5.00	-6.00	-9.00	-14.00	-19.00	-24.00
-0.80	-13.80	-12.50	-11.20	-10.10	-9.00	-10.00	-13.00	-18.00	-23.00	-28.00
-0.70	-18.80	-17.50	-16.20	-15.10	-14.00	-15.00	-18.00	-23.00	-28.00	-33.00
-0.60	-24.80	-23.50	-22.20	-21.10	-20.00	-21.00	-24.00	-29.00	-34.00	-39.00
-0.50	-30.80	-29.50	-28.20	-27.10	-26.00	-27.00	-30.00	-35.00	-40.00	-45.00
-0.40	-36.80	-35.50	-34.20	-33.10	-32.00	-33.00	-36.00	-41.00	-46.00	-51.00
-0.30	-42.80	-41.50	-40.20	-39.10	-38.00	-39.00	-42.00	-47.00	-52.00	-57.00
-0.20	-48.80	-47.50	-46.20	-45.10	-44.00	-45.00	-48.00	-53.00	-58.00	-63.00
-0.10	-54.80	-53.50	-52.20	-51.10	-50.00	-51.00	-54.00	-59.00	-64.00	-69.00
0.00	-60.80	-59.50	-58.20	-57.10	-56.00	-57.00	-60.00	-65.00	-70.00	-75.00

Table 2. Modified Stone et al[30] Low-Frequency Combustor-Noise Component (k=1) Distribution Index, continued (2)

$\log St_1$	$\theta = 0.0$	10.0	20.0	30.0	40.0	50.0	60.0	70.0	80.0	90.0
0.00	-64.30	-64.30	-64.30	-64.30	-64.30	-63.80	-63.30	-62.80	-61.80	-60.80
0.10	-70.30	-70.30	-70.30	-70.30	-70.30	-69.80	-69.30	-68.80	-67.80	-66.80
0.20	-76.30	-76.30	-76.30	-76.30	-76.30	-75.80	-75.30	-74.80	-73.80	-72.80
0.30	-82.30	-82.30	-82.30	-82.30	-82.30	-81.80	-81.30	-80.80	-79.80	-78.80
0.40	-88.30	-88.30	-88.30	-88.30	-88.30	-87.80	-87.30	-86.80	-85.80	-84.80
0.50	-94.30	-94.30	-94.30	-94.30	-94.30	-93.80	-93.30	-92.80	-91.80	-90.80
0.60	-100.30	-100.30	-100.30	-100.30	-100.30	-99.80	-99.30	-98.80	-97.80	-96.80
0.70	-106.30	-106.30	-106.30	-106.30	-106.30	-105.80	-105.30	-104.80	-103.80	-102.80
0.80	-112.30	-112.30	-112.30	-112.30	-112.30	-111.80	-111.30	-110.80	-109.80	-108.80
0.90	-118.30	-118.30	-118.30	-118.30	-118.30	-117.80	-117.30	-116.80	-115.80	-114.80
1.00	-124.30	-124.30	-124.30	-124.30	-124.30	-123.80	-123.30	-122.80	-121.80	-120.80
1.10	-130.30	-130.30	-130.30	-130.30	-130.30	-129.80	-129.30	-128.80	-127.80	-126.80
1.20	-136.30	-136.30	-136.30	-136.30	-136.30	-135.80	-135.30	-134.80	-133.80	-132.80
1.30	-142.30	-142.30	-142.30	-142.30	-142.30	-141.80	-141.30	-140.80	-139.80	-138.80
1.40	-148.30	-148.30	-148.30	-148.30	-148.30	-147.80	-147.30	-146.80	-145.80	-144.80
1.50	-154.30	-154.30	-154.30	-154.30	-154.30	-153.80	-153.30	-152.80	-151.80	-150.80
1.60	-160.30	-160.30	-160.30	-160.30	-160.30	-159.80	-159.30	-158.80	-157.80	-156.80
1.70	-166.30	-166.30	-166.30	-166.30	-166.30	-165.80	-165.30	-164.80	-163.80	-162.80
1.80	-172.30	-172.30	-172.30	-172.30	-172.30	-171.80	-171.30	-170.80	-169.80	-168.80
1.90	-178.30	-178.30	-178.30	-178.30	-178.30	-177.80	-177.30	-176.80	-175.80	-174.80
2.00	-184.30	-184.30	-184.30	-184.30	-184.30	-183.80	-183.30	-182.80	-181.80	-180.80
2.10	-190.30	-190.30	-190.30	-190.30	-190.30	-189.80	-189.30	-188.80	-187.80	-186.80
2.20	-196.30	-196.30	-196.30	-196.30	-196.30	-195.80	-195.30	-194.80	-193.80	-192.80
2.30	-202.30	-202.30	-202.30	-202.30	-202.30	-201.80	-201.30	-200.80	-199.80	-198.80
2.40	-208.30	-208.30	-208.30	-208.30	-208.30	-207.80	-207.30	-206.80	-205.80	-204.80
2.50	-214.30	-214.30	-214.30	-214.30	-214.30	-213.80	-213.30	-212.80	-211.80	-210.80
2.60	-220.30	-220.30	-220.30	-220.30	-220.30	-219.80	-219.30	-218.80	-217.80	-216.80
2.70	-226.30	-226.30	-226.30	-226.30	-226.30	-225.80	-225.30	-224.80	-223.80	222.80
2.80	-232.30	-232.30	-232.30	-232.30	-232.30	-231.80	-231.30	-230.80	-229.80	-228.80
2.90	-238.30	-238.30	-238.30	-238.30	-238.30	-237.80	-237.30	-236.80	-235.80	-234.80
3.00	-244.30	-244.30	-244.30	-244.30	-244.30	-243.80	-243.30	-242.80	-241.80	-240.80
3.10	-250.30	-250.30	-250.30	-250.30	-250.30	-249.80	-249.30	-248.80	-247.80	-246.80
3.20	-256.30	-256.30	-256.30	-256.30	-256.30	-255.80	-255.30	-254.80	-253.80	-252.80
3.30	-262.30	-262.30	-262.30	-262.30	-262.30	-261.80	-261.30	-260.80	-259.80	-258.80
3.40	-268.30	-268.30	-268.30	-268.30	-268.30	-267.80	-267.30	-266.80	-265.80	264.80
3.50	-274.30	-274.30	-274.30	-274.30	-274.30	-273.80	-273.30	-272.80	-271.80	-270.80
3.60	-280.30	-280.30	-280.30	-280.30	-280.30	-279.80	-279.30	-278.80	-277.80	-276.80
$\Delta OASPL$	-3.500	-3.500	-3.500	-3.500	-3.500	-3.000	-2.500	-2.000	-1.000	0.000

Table 2. Modified Stone et al[30] Low-Frequency Combustor-Noise Component (k=1) Distribution Index, continued (3)

$\log St_1$	$\theta = 90.0$	100.0	110.0	120.0	130.0	140.0	150.0	160.0	170.0	180.0
0.00	-60.80	-59.50	-58.20	-57.10	-56.00	-57.00	-60.00	-65.00	-70.00	-75.00
0.10	-66.80	-65.50	-64.20	-63.10	-62.00	-63.00	-66.00	-71.00	-76.00	-81.00
0.20	-72.80	-71.50	-70.20	-69.10	-68.00	-69.00	-72.00	-77.00	-82.00	-87.00
0.30	-78.80	-77.50	-76.20	-75.10	-74.00	-75.00	-78.00	-83.00	-88.00	-93.00
0.40	-84.80	-83.50	-82.20	-81.10	-80.00	-81.00	-84.00	-89.00	-94.00	-99.00
0.50	-90.80	-89.50	-88.20	-87.10	-86.00	-87.00	-90.00	-95.00	-100.00	-105.00
0.60	-96.80	-95.50	-94.20	-93.10	-92.00	-93.00	-96.00	-101.00	-106.00	-111.00
0.70	-102.80	-101.50	-100.20	-99.10	-98.00	-99.00	-102.00	-107.00	-112.00	-117.00
0.80	-108.80	-107.50	-106.20	-105.10	-104.00	-105.00	-108.00	-113.00	-118.00	-123.00
0.90	-114.80	-113.50	-112.20	-111.10	-110.00	-111.00	-114.00	-119.00	-124.00	-129.00
1.00	-120.80	-119.50	-118.20	-117.10	-116.00	-117.00	-120.00	-125.00	-130.00	-135.00
1.10	-126.80	-125.50	-124.20	-123.10	-122.00	-123.00	-126.00	-131.00	-136.00	-141.00
1.20	-132.80	-131.50	-130.20	-129.10	-128.00	-129.00	-132.00	-137.00	-142.00	-147.00
1.30	-138.80	-137.50	-136.20	-135.10	-134.00	-135.00	-138.00	-143.00	-148.00	-153.00
1.40	-144.80	-143.50	-142.20	-141.10	-140.00	-141.00	-144.00	-149.00	-154.00	-159.00
1.50	-150.80	-149.50	-148.20	-147.10	-146.00	-147.00	-150.00	-155.00	-160.00	-165.00
1.60	-156.80	-155.50	-154.20	-153.10	-152.00	-153.00	-156.00	-161.00	-166.00	-171.00
1.70	-162.80	-161.50	-160.20	-159.10	-158.00	-159.00	-162.00	-167.00	-172.00	-177.00
1.80	-168.80	-167.50	-166.20	-165.10	-164.00	-165.00	-168.00	-173.00	-178.00	-183.00
1.90	-174.80	-173.50	-172.20	-171.10	-170.00	-171.00	-174.00	-179.00	-184.00	-189.00
2.00	-180.80	-179.50	-178.20	-177.10	-176.00	-177.00	-180.00	-185.00	-190.00	-195.00
2.10	-186.80	-185.50	-184.20	-183.10	-182.00	-183.00	-186.00	-191.00	-196.00	-201.00
2.20	-192.80	-191.50	-190.20	-189.10	-188.00	-189.00	-192.00	-197.00	-202.00	-207.00
2.30	-198.80	-197.50	-196.20	-195.10	-194.00	-195.00	-198.00	-203.00	-208.00	-213.00
2.40	-204.80	-203.50	-202.20	-201.10	-200.00	-201.00	-204.00	-209.00	-214.00	-219.00
2.50	-210.80	-209.50	-208.20	-207.10	-206.00	-207.00	-210.00	-215.00	-220.00	-225.00
2.60	-216.80	-215.50	-214.20	-213.10	-212.00	-213.00	-216.00	-221.00	-226.00	-231.00
2.70	-222.80	-221.50	-220.20	-219.10	-218.00	-219.00	-222.00	-227.00	-232.00	-237.00
2.80	-228.80	-227.50	-226.20	-225.10	-224.00	-225.00	-228.00	-233.00	-238.00	-243.00
2.90	-234.80	-233.50	-232.20	-231.10	-230.00	-231.00	-234.00	-239.00	-244.00	-249.00
3.00	-240.80	-239.50	-238.20	-237.10	-236.00	-237.00	-240.00	-245.00	-250.00	-255.00
3.10	-246.80	-245.50	-244.20	-243.10	-242.00	-243.00	-246.00	-251.00	-256.00	-261.00
3.20	-252.80	-251.50	-250.20	-249.10	-248.00	-249.00	-252.00	-257.00	-262.00	-267.00
3.30	-258.80	-257.50	-256.20	-255.10	-254.00	-255.00	-258.00	-263.00	-268.00	-273.00
3.40	-264.80	-263.50	-262.20	-261.10	-260.00	-261.00	-264.00	-269.00	-274.00	-279.00
3.50	-270.80	-269.50	-268.20	-267.10	-266.00	-267.00	-270.00	-275.00	-280.00	-285.00
3.60	-276.80	-275.50	-274.20	-273.10	-272.00	-273.00	-276.00	-281.00	-286.00	-291.00
$\Delta OASPL$	0.000	1.383	2.801	4.268	5.590	4.590	1.590	-3.410	-8.410	-13.410

Table 3. Modified Stone et al[30] Mid-Frequency Combustor-Noise Component (k=2) Distribution Index

$\log St_2$	$\theta = 0.0$	10.0	20.0	30.0	40.0	50.0	60.0	70.0	80.0	90.0
-3.60	-176.31	-175.31	-174.31	-173.31	-172.31	-170.81	-169.81	-168.81	-168.31	-167.81
-3.50	-170.31	-169.31	-168.31	-167.31	-166.31	-164.81	-163.81	-162.81	-162.31	-161.81
-3.40	-164.31	-163.31	-162.31	-161.31	-160.31	-158.81	-157.81	-156.81	-156.31	-155.81
-3.30	-158.31	-157.31	-156.31	-155.31	-154.31	-152.81	-151.81	-150.81	-150.31	-149.81
-3.20	-152.31	-151.31	-150.31	-149.31	-148.31	-146.81	-145.81	-144.81	-144.31	-143.81
-3.10	-146.31	-145.31	-144.31	-143.31	-142.31	-140.81	-139.81	-138.81	-138.31	-137.81
-3.00	-140.31	-139.31	-138.31	-137.31	-136.31	-134.81	-133.81	-132.81	-132.31	-131.81
-2.90	-134.31	-133.31	-132.31	-131.31	-130.31	-128.81	-127.81	-126.81	-126.31	-125.81
-2.80	-128.31	-127.31	-126.31	-125.31	-124.31	-122.81	-121.81	-120.81	-120.31	-119.81
-2.70	-122.31	-121.31	-120.31	-119.31	-118.31	-116.81	-115.81	-114.81	-114.31	-113.81
-2.60	-116.31	-115.31	-114.31	-113.31	-112.31	-110.81	-109.81	-108.81	-108.31	-107.81
-2.50	-110.31	-109.31	-108.31	-107.31	-106.31	-104.81	-103.81	-102.81	-102.31	-101.81
-2.40	-104.31	-103.31	-102.31	-101.31	-100.31	-98.81	-97.81	-96.81	-96.31	-95.81
-2.30	-98.31	-97.31	-96.31	-95.31	-94.31	-92.81	-91.81	-90.81	-90.31	-89.81
-2.20	-92.31	-91.31	-90.31	-89.31	-88.31	-86.81	-85.81	-84.81	-84.31	-83.81
-2.10	-86.31	-85.31	-84.31	-83.31	-82.31	-80.81	-79.81	-78.81	-78.31	-77.81
-2.00	-80.31	-79.31	-78.31	-77.31	-76.31	-74.81	-73.81	-72.81	-72.31	-71.81
-1.90	-74.31	-73.31	-72.31	-71.31	-70.31	-68.81	-67.81	-66.81	-66.31	-65.81
-1.80	-68.31	-67.31	-66.31	-65.31	-64.31	-62.81	-61.81	-60.81	-60.31	-59.81
-1.70	-62.31	-61.31	-60.31	-59.31	-58.31	-56.81	-55.81	-54.81	-54.31	-53.81
-1.60	-56.31	-55.31	-54.31	-53.31	-52.31	-50.81	-49.81	-48.81	-48.31	-47.81
-1.50	-50.31	-49.31	-48.31	-47.31	-46.31	-44.81	-43.81	-42.81	-42.31	-41.81
-1.40	-44.31	-43.31	-42.31	-41.31	-40.31	-38.81	-37.81	-36.81	-36.31	-35.81
-1.30	-38.31	-37.31	-36.31	-35.31	-34.31	-32.81	-31.81	-30.81	-30.31	-29.81
-1.20	-32.31	-31.31	-30.31	-29.31	-28.31	-26.81	-25.81	-24.81	-24.31	-23.81
-1.10	-26.31	-25.31	-24.31	-23.31	-22.31	-20.81	-19.81	-18.81	-18.31	-17.81
-1.00	-20.31	-19.31	-18.31	-17.31	-16.31	-14.81	-13.81	-12.81	-12.31	-11.81
-0.90	-16.31	-15.31	-14.31	-13.31	-12.31	-10.81	-9.81	-8.81	-8.31	-7.81
-0.80	-14.31	-13.31	-12.31	-11.31	-10.31	-8.81	-7.81	-6.81	-6.31	-5.81
-0.70	-15.01	-14.01	-13.01	-12.01	-11.01	-9.51	-8.51	-7.51	-7.01	-6.51
-0.60	-16.91	-15.91	-14.91	-13.91	-12.91	-11.41	-10.41	-9.41	-8.91	-8.41
-0.50	-19.81	-18.81	-17.81	-16.81	-15.81	-14.31	-13.31	-12.31	-11.81	-11.31
-0.40	-23.81	-22.81	-21.81	-20.81	-19.81	-18.31	-17.31	-16.31	-15.81	-15.31
-0.30	-28.81	-27.81	-26.81	-25.81	-24.81	-23.31	-22.31	-21.31	-20.81	-20.31
-0.20	-34.11	-33.11	-32.11	-31.11	-30.11	-28.61	-27.61	-26.61	-26.11	-25.61
-0.10	-39.71	-38.71	-37.71	-36.71	-35.71	-34.21	-33.21	-32.21	-31.71	-31.21
0.00	-45.71	-44.71	-43.71	-42.71	-41.71	-40.21	-39.21	-38.21	-37.71	-37.21

Table 3. Modified Stone et al[30] Mid-Frequency Combustor-Noise Component (k=2) Distribution Index, continued (1)

$\log St_2$	$\theta = 90.0$	100.0	110.0	120.0	130.0	140.0	150.0	160.0	170.0	180.0
-3.60	-167.81	-167.31	-166.81	-166.31	-165.81	-167.31	-169.51	-171.71	-173.91	-176.11
-3.50	-161.81	-161.31	-160.81	-160.31	-159.81	-161.31	-163.51	-165.71	-167.91	-170.11
-3.40	-155.81	-155.31	-154.81	-154.31	-153.81	-155.31	-157.51	-159.71	-161.91	-164.11
-3.30	-149.81	-149.31	-148.81	-148.31	-147.81	-149.31	-151.51	-153.71	-155.91	-158.11
-3.20	-143.81	-143.31	-142.81	-142.31	-141.81	-143.31	-145.51	-147.71	-149.91	-152.11
-3.10	-137.81	-137.31	-136.81	-136.31	-135.81	-137.31	-139.51	-141.71	-143.91	-146.11
-3.00	-131.81	-131.31	-130.81	-130.31	-129.81	-131.31	-133.51	-135.71	-137.91	-140.11
-2.90	-125.81	-125.31	-124.81	-124.31	-123.81	-125.31	-127.51	-129.71	-131.91	-134.11
-2.80	-119.81	-119.31	-118.81	-118.31	-117.81	-119.31	-121.51	-123.71	-125.91	-128.11
-2.70	-113.81	-113.31	-112.81	-112.31	-111.81	-113.31	-115.51	-117.71	-119.91	-122.11
-2.60	-107.81	-107.31	-106.81	-106.31	-105.81	-107.31	-109.51	-111.71	-113.91	-116.11
-2.50	-101.81	-101.31	-100.81	-100.31	-99.81	-101.31	-103.51	-105.71	-107.91	-110.11
-2.40	-95.81	-95.31	-94.81	-94.31	-93.81	-95.31	-97.51	-99.71	-101.91	-104.11
-2.30	-89.81	-89.31	-88.81	-88.31	-87.81	-89.31	-91.51	-93.71	-95.91	-98.11
-2.20	-83.81	-83.31	-82.81	-82.31	-81.81	-83.31	-85.51	-87.71	-89.91	-92.11
-2.10	-77.81	-77.31	-76.81	-76.31	-75.81	-77.31	-79.51	-81.71	-83.91	-86.11
-2.00	-71.81	-71.31	-70.81	-70.31	-69.81	-71.31	-73.51	-75.71	-77.91	-80.11
-1.90	-65.81	-65.31	-64.81	-64.31	-63.81	-65.31	-67.51	-69.71	-71.91	-74.11
-1.80	-59.81	-59.31	-58.81	-58.31	-57.81	-59.31	-61.51	-63.71	-65.91	-68.11
-1.70	-53.81	-53.31	-52.81	-52.31	-51.81	-53.31	-55.51	-57.71	-59.91	-62.11
-1.60	-47.81	-47.31	-46.81	-46.31	-45.81	-47.31	-49.51	-51.71	-53.91	-56.11
-1.50	-41.81	-41.31	-40.81	-40.31	-39.81	-41.31	-43.51	-45.71	-47.91	-50.11
-1.40	-35.81	-35.31	-34.81	-34.31	-33.81	-35.31	-37.51	-39.71	-41.91	-44.11
-1.30	-29.81	-29.31	-28.81	-28.31	-27.81	-29.31	-31.51	-33.71	-35.91	-38.11
-1.20	-23.81	-23.31	-22.81	-22.31	-21.81	-23.31	-25.51	-27.71	-29.91	-32.11
-1.10	-17.81	-17.31	-16.81	-16.31	-15.81	-17.31	-19.51	-21.71	-23.91	-26.11
-1.00	-11.81	-11.31	-10.81	-10.31	-9.81	-11.31	-13.51	-15.71	-17.91	-20.11
-0.90	-7.81	-7.31	-6.81	-6.31	-5.81	-7.31	-9.51	-11.71	-13.91	-16.11
-0.80	-5.81	-5.31	-4.81	-4.31	-3.81	-5.31	-7.51	-9.71	-11.91	-14.11
-0.70	-6.51	-6.01	-5.51	-5.01	-4.51	-6.01	-8.21	-10.41	-12.61	-14.81
-0.60	-8.41	-7.91	-7.41	-6.91	-6.41	-7.91	-10.11	-12.31	-14.51	-16.71
-0.50	-11.31	-10.81	-10.31	-9.81	-9.31	-10.81	-13.01	-15.21	-17.41	-19.61
-0.40	-15.31	-14.81	-14.31	-13.81	-13.31	-14.81	-17.01	-19.21	-21.41	-23.61
-0.30	-20.31	-19.81	-19.31	-18.81	-18.31	-19.81	-22.01	-24.21	-26.41	-28.61
-0.20	-25.61	-25.11	-24.61	-24.11	-23.61	-25.11	-27.31	-29.51	-31.71	-33.91
-0.10	-31.21	-30.71	-30.21	-29.71	-29.21	-30.71	-32.91	-35.11	-37.31	-39.51
0.00	-37.21	-36.71	-36.21	-35.71	-35.21	-36.71	-38.91	-41.11	-43.31	-45.51

Table 3. Modified Stone et al[30] Mid-Frequency Combustor-Noise Component (k=2) Distribution Index, continued (2)

$\log St_2$	$\theta = 0.0$	10.0	20.0	30.0	40.0	50.0	60.0	70.0	80.0	90.0
0.00	-45.71	-44.71	-43.71	-42.71	-41.71	-40.21	-39.21	-38.21	-37.71	-37.21
0.10	-51.71	-50.71	-49.71	-48.71	-47.71	-46.21	-45.21	-44.21	-43.71	-43.21
0.20	-57.71	-56.71	-55.71	-54.71	-53.71	-52.21	-51.21	-50.21	-49.71	-49.21
0.30	-63.71	-62.71	-61.71	-60.71	-59.71	-58.21	-57.21	-56.21	-55.71	-55.21
0.40	-69.71	-68.71	-67.71	-66.71	-65.71	-64.21	-63.21	-62.21	-61.71	-61.21
0.50	-75.71	-74.71	-73.71	-72.71	-71.71	-70.21	-69.21	-68.21	-67.71	-67.21
0.60	-81.71	-80.71	-79.71	-78.71	-77.71	-76.21	-75.21	-74.21	-73.71	-73.21
0.70	-87.71	-86.71	-85.71	-84.71	-83.71	-82.21	-81.21	-80.21	-79.71	-79.21
0.80	-93.71	-92.71	-91.71	-90.71	-89.71	-88.21	-87.21	-86.21	-85.71	-85.21
0.90	-99.71	-98.71	-97.71	-96.71	-95.71	-94.21	-93.21	-92.21	-91.71	-91.21
1.00	-105.71	-104.71	-103.71	-102.71	-101.71	-100.21	-99.21	-98.21	-97.71	-97.21
1.10	-111.71	-110.71	-109.71	-108.71	-107.71	-106.21	-105.21	-104.21	-103.71	-103.21
1.20	-117.71	-116.71	-115.71	-114.71	-113.71	-112.21	-111.21	-110.21	-109.71	-109.21
1.30	-123.71	-122.71	-121.71	-120.71	-119.71	-118.21	-117.21	-116.21	-115.71	-115.21
1.40	-129.71	-128.71	-127.71	-126.71	-125.71	-124.21	-123.21	-122.21	-121.71	-121.21
1.50	-135.71	-134.71	-133.71	-132.71	-131.71	-130.21	-129.21	-128.21	-127.71	-127.21
1.60	-141.71	-140.71	-139.71	-138.71	-137.71	-136.21	-135.21	-134.21	-133.71	-133.21
1.70	-147.71	-146.71	-145.71	-144.71	-143.71	-142.21	-141.21	-140.21	-139.71	-139.21
1.80	-153.71	-152.71	-151.71	-150.71	-149.71	-148.21	-147.21	-146.21	-145.71	-145.21
1.90	-159.71	-158.71	-157.71	-156.71	-155.71	-154.21	-153.21	-152.21	-151.71	-151.21
2.00	-165.71	-164.71	-163.71	-162.71	-161.71	-160.21	-159.21	-158.21	-157.71	-157.21
2.10	-171.71	-170.71	-169.71	-168.71	-167.71	-166.21	-165.21	-164.21	-163.71	-163.21
2.20	-177.71	-176.71	-175.71	-174.71	-173.71	-172.21	-171.21	-170.21	-169.71	-169.21
2.30	-183.71	-182.71	-181.71	-180.71	-179.71	-178.21	-177.21	-176.21	-175.71	-175.21
2.40	-189.71	-188.71	-187.71	-186.71	-185.71	-184.21	-183.21	-182.21	-181.71	-181.21
2.50	-195.71	-194.71	-193.71	-192.71	-191.71	-190.21	-189.21	-188.21	-187.71	-187.21
2.60	-201.71	-200.71	-199.71	-198.71	-197.71	-196.21	-195.21	-194.21	-193.71	-193.21
2.70	-207.71	-206.71	-205.71	-204.71	-203.71	-202.21	-201.21	-200.21	-199.71	-199.21
2.80	-213.71	-212.71	-211.71	-210.71	-209.71	-208.21	-207.21	-206.21	-205.71	-205.21
2.90	-219.71	-218.71	-217.71	-216.71	-215.71	-214.21	-213.21	-212.21	-211.71	-211.21
3.00	-225.71	-224.71	-223.71	-222.71	-221.71	-220.21	-219.21	-218.21	-217.71	-217.21
3.10	-231.71	-230.71	-229.71	-228.71	-227.71	-226.21	-225.21	-224.21	-223.71	-223.21
3.20	-237.71	-236.71	-235.71	-234.71	-233.71	-232.21	-231.21	-230.21	-229.71	-229.21
3.30	-243.71	-242.71	-241.71	-240.71	-239.71	-238.21	-237.21	-236.21	-235.71	-235.21
3.40	-249.71	-248.71	-247.71	-246.71	-245.71	-244.21	-243.21	-242.21	-241.71	-241.21
3.50	-255.71	-254.71	-253.71	-252.71	-251.71	-250.21	-249.21	-248.21	-247.71	-247.21
3.60	-261.71	-260.71	-259.71	-258.71	-257.71	-256.21	-255.21	-254.21	-253.71	-253.21
$\Delta OASPL$	-8.500	-7.500	-6.500	-5.500	-4.500	-3.000	-2.000	-1.000	-0.500	0.000

Table 3. Modified Stone et al[30] Mid-Frequency Combustor-Noise Component (k=2) Distribution Index, continued (3)

$\log St_2$	$\theta = 90.0$	100.0	110.0	120.0	130.0	140.0	150.0	160.0	170.0	180.0
0.00	-37.21	-36.71	-36.21	-35.71	-35.21	-36.71	-38.91	-41.11	-43.31	-45.51
0.10	-43.21	-42.71	-42.21	-41.71	-41.21	-42.71	-44.91	-47.11	-49.31	-51.51
0.20	-49.21	-48.71	-48.21	-47.71	-47.21	-48.71	-50.91	-53.11	-55.31	-57.51
0.30	-55.21	-54.71	-54.21	-53.71	-53.21	-54.71	-56.91	-59.11	-61.31	-63.51
0.40	-61.21	-60.71	-60.21	-59.71	-59.21	-60.71	-62.91	-65.11	-67.31	-69.51
0.50	-67.21	-66.71	-66.21	-65.71	-65.21	-66.71	-68.91	-71.11	-73.31	-75.51
0.60	-73.21	-72.71	-72.21	-71.71	-71.21	-72.71	-74.91	-77.11	-79.31	-81.51
0.70	-79.21	-78.71	-78.21	-77.71	-77.21	-78.71	-80.91	-83.11	-85.31	-87.51
0.80	-85.21	-84.71	-84.21	-83.71	-83.21	-84.71	-86.91	-89.11	-91.31	-93.51
0.90	-91.21	-90.71	-90.21	-89.71	-89.21	-90.71	-92.91	-95.11	-97.31	-99.51
1.00	-97.21	-96.71	-96.21	-95.71	-95.21	-96.71	-98.91	-101.11	-103.31	-105.51
1.10	-103.21	-102.71	-102.21	-101.71	-101.21	-102.71	-104.91	-107.11	-109.31	-111.51
1.20	-109.21	-108.71	-108.21	-107.71	-107.21	-108.71	-110.91	-113.11	-115.31	-117.51
1.30	-115.21	-114.71	-114.21	-113.71	-113.21	-114.71	-116.91	-119.11	-121.31	-123.51
1.40	-121.21	-120.71	-120.21	-119.71	-119.21	-120.71	-122.91	-125.11	-127.31	-129.51
1.50	-127.21	-126.71	-126.21	-125.71	-125.21	-126.71	-128.91	-131.11	-133.31	-135.51
1.60	-133.21	-132.71	-132.21	-131.71	-131.21	-132.71	-134.91	-137.11	-139.31	-141.51
1.70	-139.21	-138.71	-138.21	-137.71	-137.21	-138.71	-140.91	-143.11	-145.31	-147.51
1.80	-145.21	-144.71	-144.21	-143.71	-143.21	-144.71	-146.91	-149.11	-151.31	-153.51
1.90	-151.21	-150.71	-150.21	-149.71	-149.21	-150.71	-152.91	-155.11	-157.31	-159.51
2.00	-157.21	-156.71	-156.21	-155.71	-155.21	-156.71	-158.91	-161.11	-163.31	-165.51
2.10	-163.21	-162.71	-162.21	-161.71	-161.21	-162.71	-164.91	-167.11	-169.31	-171.51
2.20	-169.21	-168.71	-168.21	-167.71	-167.21	-168.71	-170.91	-173.11	-175.31	-177.51
2.30	-175.21	-174.71	-174.21	-173.71	-173.21	-174.71	-176.91	-179.11	-181.31	-183.51
2.40	-181.21	-180.71	-180.21	-179.71	-179.21	-180.71	-182.91	-185.11	-187.31	-189.51
2.50	-187.21	-186.71	-186.21	-185.71	-185.21	-186.71	-188.91	-191.11	-193.31	-195.51
2.60	-193.21	-192.71	-192.21	-191.71	-191.21	-192.71	-194.91	-197.11	-199.31	-201.51
2.70	-199.21	-198.71	-198.21	-197.71	-197.21	-198.71	-200.91	-203.11	-205.31	-207.51
2.80	-205.21	-204.71	-204.21	-203.71	-203.21	-204.71	-206.91	-209.11	-211.31	-213.51
2.90	-211.21	-210.71	-210.21	-209.71	-209.21	-210.71	-212.91	-215.11	-217.31	-219.51
3.00	-217.21	-216.71	-216.21	-215.71	-215.21	-216.71	-218.91	-221.11	-223.31	-225.51
3.10	-223.21	-222.71	-222.21	-221.71	-221.21	-222.71	-224.91	-227.11	-229.31	-231.51
3.20	-229.21	-228.71	-228.21	-227.71	-227.21	-228.71	-230.91	-233.11	-235.31	-237.51
3.30	-235.21	-234.71	-234.21	-233.71	-233.21	-234.71	-236.91	-239.11	-241.31	-243.51
3.40	-241.21	-240.71	-240.21	-239.71	-239.21	-240.71	-242.91	-245.11	-247.31	-249.51
3.50	-247.21	-246.71	-246.21	-245.71	-245.21	-246.71	-248.91	-251.11	-253.31	-255.51
3.60	-253.21	-252.71	-252.21	-251.71	-251.21	-252.71	-254.91	-257.11	-259.31	-261.51
$\Delta OASPL$	0.000	0.500	1.000	1.500	2.000	0.500	-1.700	-3.900	-6.100	-8.300

Table 4. Modified Stone et al[30] High-Frequency Combustor-Noise Component (k=3) Distribution Index

$\log St_3$	$\theta = 0.0$	10.0	20.0	30.0	40.0	50.0	60.0	70.0	80.0	90.0
-3.60	-199.24	-198.64	-198.04	-197.44	-196.84	-196.14	-195.44	-195.24	-194.84	-194.04
-3.50	-193.24	-192.64	-192.04	-191.44	-190.84	-190.14	-189.44	-189.24	-188.84	-188.04
-3.40	-187.24	-186.64	-186.04	-185.44	-184.84	-184.14	-183.44	-183.24	-182.84	-182.04
-3.30	-181.24	-180.64	-180.04	-179.44	-178.84	-178.14	-177.44	-177.24	-176.84	-176.04
-3.20	-175.24	-174.64	-174.04	-173.44	-172.84	-172.14	-171.44	-171.24	-170.84	-170.04
-3.10	-169.24	-168.64	-168.04	-167.44	-166.84	-166.14	-165.44	-165.24	-164.84	-164.04
-3.00	-163.24	-162.64	-162.04	-161.44	-160.84	-160.14	-159.44	-159.24	-158.84	-158.04
-2.90	-157.24	-156.64	-156.04	-155.44	-154.84	-154.14	-153.44	-153.24	-152.84	-152.04
-2.80	-151.24	-150.64	-150.04	-149.44	-148.84	-148.14	-147.44	-147.24	-146.84	-146.04
-2.70	-145.24	-144.64	-144.04	-143.44	-142.84	-142.14	-141.44	-141.24	-140.84	-140.04
-2.60	-139.24	-138.64	-138.04	-137.44	-136.84	-136.14	-135.44	-135.24	-134.84	-134.04
-2.50	-133.24	-132.64	-132.04	-131.44	-130.84	-130.14	-129.44	-129.24	-128.84	-128.04
-2.40	-127.24	-126.64	-126.04	-125.44	-124.84	-124.14	-123.44	-123.24	-122.84	-122.04
-2.30	-121.24	-120.64	-120.04	-119.44	-118.84	-118.14	-117.44	-117.24	-116.84	-116.04
-2.20	-115.24	-114.64	-114.04	-113.44	-112.84	-112.14	-111.44	-111.24	-110.84	-110.04
-2.10	-109.24	-108.64	-108.04	-107.44	-106.84	-106.14	-105.44	-105.24	-104.84	-104.04
-2.00	-103.24	-102.64	-102.04	-101.44	-100.84	-100.14	-99.44	-99.24	-98.84	-98.04
-1.90	-97.24	-96.64	-96.04	-95.44	-94.84	-94.14	-93.44	-93.24	-92.84	-92.04
-1.80	-91.24	-90.64	-90.04	-89.44	-88.84	-88.14	-87.44	-87.24	-86.84	-86.04
-1.70	-85.24	-84.64	-84.04	-83.44	-82.84	-82.14	-81.44	-81.24	-80.84	-80.04
-1.60	-79.24	-78.64	-78.04	-77.44	-76.84	-76.14	-75.44	-75.24	-74.84	-74.04
-1.50	-73.24	-72.64	-72.04	-71.44	-70.84	-70.14	-69.44	-69.24	-68.84	-68.04
-1.40	-67.24	-66.64	-66.04	-65.44	-64.84	-64.14	-63.44	-63.24	-62.84	-62.04
-1.30	-61.24	-60.64	-60.04	-59.44	-58.84	-58.14	-57.44	-57.24	-56.84	-56.04
-1.20	-55.24	-54.64	-54.04	-53.44	-52.84	-52.14	-51.44	-51.24	-50.84	-50.04
-1.10	-49.24	-48.64	-48.04	-47.44	-46.84	-46.14	-45.44	-45.24	-44.84	-44.04
-1.00	-43.24	-42.64	-42.04	-41.44	-40.84	-40.14	-39.44	-39.24	-38.84	-38.04
-0.90	-37.24	-36.64	-36.04	-35.44	-34.84	-34.14	-33.44	-33.24	-32.84	-32.04
-0.80	-31.24	-30.64	-30.04	-29.44	-28.84	-28.14	-27.44	-27.24	-26.84	-26.04
-0.70	-25.24	-24.64	-24.04	-23.44	-22.84	-22.14	-21.44	-21.24	-20.84	-20.04
-0.60	-20.04	-19.44	-18.84	-18.24	-17.64	-16.94	-16.24	-16.04	-15.64	-14.84
-0.50	-15.94	-15.34	-14.74	-14.14	-13.54	-12.84	-12.14	-11.94	-11.54	-10.74
-0.40	-13.04	-12.44	-11.84	-11.24	-10.64	-9.94	-9.24	-9.04	-8.64	-7.84
-0.30	-12.04	-11.44	-10.84	-10.24	-9.64	-8.94	-8.24	-8.04	-7.64	-6.84
-0.20	-12.34	-11.74	-11.14	-10.54	-9.94	-9.24	-8.54	-8.34	-7.94	-7.14
-0.10	-13.34	-12.74	-12.14	-11.54	-10.94	-10.24	-9.54	-9.34	-8.94	-8.14
0.00	-15.54	-14.94	-14.34	-13.74	-13.14	-12.44	-11.74	-11.54	-11.14	-10.34

Table 4. Modified Stone et al[30] High-Frequency Combustor-Noise Component (k=3) Distribution Index, continued (1)

$\log St_3$	$\theta = 90.0$	100.0	110.0	120.0	130.0	140.0	150.0	160.0	170.0	180.0
-3.60	-194.04	-192.54	-190.84	-189.04	-187.64	-191.14	-193.64	-195.64	-197.64	-199.64
-3.50	-188.04	-186.54	-184.84	-183.04	-181.64	-185.14	-187.64	-189.64	-191.64	-193.64
-3.40	-182.04	-180.54	-178.84	-177.04	-175.64	-179.14	-181.64	-183.64	-185.64	-187.64
-3.30	-176.04	-174.54	-172.84	-171.04	-169.64	-173.14	-175.64	-177.64	-179.64	-181.64
-3.20	-170.04	-168.54	-166.84	-165.04	-163.64	-167.14	-169.64	-171.64	-173.64	-175.64
-3.10	-164.04	-162.54	-160.84	-159.04	-157.64	-161.14	-163.64	-165.64	-167.64	-169.64
-3.00	-158.04	-156.54	-154.84	-153.04	-151.64	-155.14	-157.64	-159.64	-161.64	-163.64
-2.90	-152.04	-150.54	-148.84	-147.04	-145.64	-149.14	-151.64	-153.64	-155.64	-157.64
-2.80	-146.04	-144.54	-142.84	-141.04	-139.64	-143.14	-145.64	-147.64	-149.64	-151.64
-2.70	-140.04	-138.54	-136.84	-135.04	-133.64	-137.14	-139.64	-141.64	-143.64	-145.64
-2.60	-134.04	-132.54	-130.84	-129.04	-127.64	-131.14	-133.64	-135.64	-137.64	-139.64
-2.50	-128.04	-126.54	-124.84	-123.04	-121.64	-125.14	-127.64	-129.64	-131.64	-133.64
-2.40	-122.04	-120.54	-118.84	-117.04	-115.64	-119.14	-121.64	-123.64	-125.64	-127.64
-2.30	-116.04	-114.54	-112.84	-111.04	-109.64	-113.14	-115.64	-117.64	-119.64	-121.64
-2.20	-110.04	-108.54	-106.84	-105.04	-103.64	-107.14	-109.64	-111.64	-113.64	-115.64
-2.10	-104.04	-102.54	-100.84	-99.04	-97.64	-101.14	-103.64	-105.64	-107.64	-109.64
-2.00	-98.04	-96.54	-94.84	-93.04	-91.64	-95.14	-97.64	-99.64	-101.64	-103.64
-1.90	-92.04	-90.54	-88.84	-87.04	-85.64	-89.14	-91.64	-93.64	-95.64	-97.64
-1.80	-86.04	-84.54	-82.84	-81.04	-79.64	-83.14	-85.64	-87.64	-89.64	-91.64
-1.70	-80.04	-78.54	-76.84	-75.04	-73.64	-77.14	-79.64	-81.64	-83.64	-85.64
-1.60	-74.04	-72.54	-70.84	-69.04	-67.64	-71.14	-73.64	-75.64	-77.64	-79.64
-1.50	-68.04	-66.54	-64.84	-63.04	-61.64	-65.14	-67.64	-69.64	-71.64	-73.64
-1.40	-62.04	-60.54	-58.84	-57.04	-55.64	-59.14	-61.64	-63.64	-65.64	-67.64
-1.30	-56.04	-54.54	-52.84	-51.04	-49.64	-53.14	-55.64	-57.64	-59.64	-61.64
-1.20	-50.04	-48.54	-46.84	-45.04	-43.64	-47.14	-49.64	-51.64	-53.64	-55.64
-1.10	-44.04	-42.54	-40.84	-39.04	-37.64	-41.14	-43.64	-45.64	-47.64	-49.64
-1.00	-38.04	-36.54	-34.84	-33.04	-31.64	-35.14	-37.64	-39.64	-41.64	-43.64
-0.90	-32.04	-30.54	-28.84	-27.04	-25.64	-29.14	-31.64	-33.64	-35.64	-37.64
-0.80	-26.04	-24.54	-22.84	-21.04	-19.64	-23.14	-25.64	-27.64	-29.64	-31.64
-0.70	-20.04	-18.54	-16.84	-15.04	-13.64	-17.14	-19.64	-21.64	-23.64	-25.64
-0.60	-14.84	-13.34	-11.64	-9.84	-8.44	-11.94	-14.44	-16.44	-18.44	-20.44
-0.50	-10.74	-9.24	-7.54	-5.74	-4.34	-7.84	-10.34	-12.34	-14.34	-16.34
-0.40	-7.84	-6.34	-4.64	-2.84	-1.44	-4.94	-7.44	-9.44	-11.44	-13.44
-0.30	-6.84	-5.34	-3.64	-1.84	-0.44	-3.94	-6.44	-8.44	-10.44	-12.44
-0.20	-7.14	-5.64	-3.94	-2.14	-0.74	-4.24	-6.74	-8.74	-11.14	-13.14
-0.10	-8.14	-6.64	-4.94	-3.14	-1.74	-5.24	-7.74	-9.74	-12.64	-14.64
0.00	-10.34	-8.84	-7.14	-5.34	-3.94	-7.44	-9.94	-11.94	-15.44	-17.44

Table 4. Modified Stone et al[30] High-Frequency Combustor-Noise Component (k=3) Distribution Index, continued (2)

$\log St_3$	$\theta = 0.0$	10.0	20.0	30.0	40.0	50.0	60.0	70.0	80.0	90.0
0.00	-15.54	-14.94	-14.34	-13.74	-13.14	-12.44	-11.74	-11.54	-11.14	-10.34
0.10	-19.14	-18.54	-17.94	-17.34	-16.74	-16.04	-15.34	-15.14	-14.74	-13.94
0.20	-23.64	-23.04	-22.44	-21.84	-21.24	-20.54	-19.84	-19.64	-19.24	-18.44
0.30	-29.64	-29.04	-28.44	-27.84	-27.24	-26.54	-25.84	-25.64	-25.24	-24.44
0.40	-35.64	-35.04	-34.44	-33.84	-33.24	-32.54	-31.84	-31.64	-31.24	-30.44
0.50	-41.64	-41.04	-40.44	-39.84	-39.24	-38.54	-37.84	-37.64	-37.24	-36.44
0.60	-47.64	-47.04	-46.44	-45.84	-45.24	-44.54	-43.84	-43.64	-43.24	-42.44
0.70	-53.64	-53.04	-52.44	-51.84	-51.24	-50.54	-49.84	-49.64	-49.24	-48.44
0.80	-59.64	-59.04	-58.44	-57.84	-57.24	-56.54	-55.84	-55.64	-55.24	-54.44
0.90	-65.64	-65.04	-64.44	-63.84	-63.24	-62.54	-61.84	-61.64	-61.24	-60.44
1.00	-71.64	-71.04	-70.44	-69.84	-69.24	-68.54	-67.84	-67.64	-67.24	-66.44
1.10	-77.64	-77.04	-76.44	-75.84	-75.24	-74.54	-73.84	-73.64	-73.24	-72.44
1.20	-83.64	-83.04	-82.44	-81.84	-81.24	-80.54	-79.84	-79.64	-79.24	-78.44
1.30	-89.64	-89.04	-88.44	-87.84	-87.24	-86.54	-85.84	-85.64	-85.24	-84.44
1.40	-95.64	-95.04	-94.44	-93.84	-93.24	-92.54	-91.84	-91.64	-91.24	-90.44
1.50	-101.64	-101.04	-100.44	-99.84	-99.24	-98.54	-97.84	-97.64	-97.24	-96.44
1.60	-107.64	-107.04	-106.44	-105.84	-105.24	-104.54	-103.84	-103.64	-103.24	-102.44
1.70	-113.64	-113.04	-112.44	-111.84	-111.24	-110.54	-109.84	-109.64	-109.24	-108.44
1.80	-119.64	-119.04	-118.44	-117.84	-117.24	-116.54	-115.84	-115.64	-115.24	-114.44
1.90	-125.64	-125.04	-124.44	-123.84	-123.24	-122.54	-121.84	-121.64	-121.24	-120.44
2.00	-131.64	-131.04	-130.44	-129.84	-129.24	-128.54	-127.84	-127.64	-127.24	-126.44
2.10	-137.64	-137.04	-136.44	-135.84	-135.24	-134.54	-133.84	-133.64	-133.24	-132.44
2.20	-143.64	-143.04	-142.44	-141.84	-141.24	-140.54	-139.84	-139.64	-139.24	-138.44
2.30	-149.64	-149.04	-148.44	-147.84	-147.24	-146.54	-145.84	-145.64	-145.24	-144.44
2.40	-155.64	-155.04	-154.44	-153.84	-153.24	-152.54	-151.84	-151.64	-151.24	-150.44
2.50	-161.64	-161.04	-160.44	-159.84	-159.24	-158.54	-157.84	-157.64	-157.24	-156.44
2.60	-167.64	-167.04	-166.44	-165.84	-165.24	-164.54	-163.84	-163.64	-163.24	-162.44
2.70	-173.64	-173.04	-172.44	-171.84	-171.24	-170.54	-169.84	-169.64	-169.24	-168.44
2.80	-179.64	-179.04	-178.44	-177.84	-177.24	-176.54	-175.84	-175.64	-175.24	-174.44
2.90	-185.64	-185.04	-184.44	-183.84	-183.24	-182.54	-181.84	-181.64	-181.24	-180.44
3.00	-191.64	-191.04	-190.44	-189.84	-189.24	-188.54	-187.84	-187.64	-187.24	-186.44
3.10	-197.64	-197.04	-196.44	-195.84	-195.24	-194.54	-193.84	-193.64	-193.24	-192.44
3.20	-203.64	-203.04	-202.44	-201.84	-201.24	-200.54	-199.84	-199.64	-199.24	-198.44
3.30	-209.64	-209.04	-208.44	-207.84	-207.24	-206.54	-205.84	-205.64	-205.24	-204.44
3.40	-215.64	-215.04	-214.44	-213.84	-213.24	-212.54	-211.84	-211.64	-211.24	-210.44
3.50	-221.64	-221.04	-220.44	-219.84	-219.24	-218.54	-217.84	-217.64	-217.24	-216.44
3.60	-227.64	-227.04	-226.44	-225.84	-225.24	-224.54	-223.84	-223.64	-223.24	-222.44
$\Delta OASPL$	-5.200	-4.600	-4.000	-3.400	-2.800	-2.100	-1.400	-1.200	-0.800	0.000

Table 4. Modified Stone et al[30] High-Frequency Combustor-Noise Component (k=3) Distribution Index, continued (3)

$\log St_3$	$\theta = 90.0$	100.0	110.0	120.0	130.0	140.0	150.0	160.0	170.0	180.0
0.00	-10.34	-8.84	-7.14	-5.34	-3.94	-7.44	-9.94	-11.94	-15.44	-17.44
0.10	-13.94	-12.44	-10.74	-8.94	-7.54	-11.04	-13.54	-15.54	-19.74	-21.74
0.20	-18.44	-16.94	-15.24	-13.44	-12.04	-15.54	-18.04	-20.04	-25.54	-27.54
0.30	-24.44	-22.94	-21.24	-19.44	-18.04	-21.54	-24.04	-26.04	-31.54	-33.54
0.40	-30.44	-28.94	-27.24	-25.44	-24.04	-27.54	-30.04	-32.04	-37.54	-39.54
0.50	-36.44	-34.94	-33.24	-31.44	-30.04	-33.54	-36.04	-38.04	-43.54	-45.54
0.60	-42.44	-40.94	-39.24	-37.44	-36.04	-39.54	-42.04	-44.04	-49.54	-51.54
0.70	-48.44	-46.94	-45.24	-43.44	-42.04	-45.54	-48.04	-50.04	-55.54	-57.54
0.80	-54.44	-52.94	-51.24	-49.44	-48.04	-51.54	-54.04	-56.04	-61.54	-63.54
0.90	-60.44	-58.94	-57.24	-55.44	-54.04	-57.54	-60.04	-62.04	-67.54	-69.54
1.00	-66.44	-64.94	-63.24	-61.44	-60.04	-63.54	-66.04	-68.04	-73.54	-75.54
1.10	-72.44	-70.94	-69.24	-67.44	-66.04	-69.54	-72.04	-74.04	-79.54	-81.54
1.20	-78.44	-76.94	-75.24	-73.44	-72.04	-75.54	-78.04	-80.04	-85.54	-87.54
1.30	-84.44	-82.94	-81.24	-79.44	-78.04	-81.54	-84.04	-86.04	-91.54	-93.54
1.40	-90.44	-88.94	-87.24	-85.44	-84.04	-87.54	-90.04	-92.04	-97.54	-99.54
1.50	-96.44	-94.94	-93.24	-91.44	-90.04	-93.54	-96.04	-98.04	-103.54	-105.54
1.60	-102.44	-100.94	-99.24	-97.44	-96.04	-99.54	-102.04	-104.04	-109.54	-111.54
1.70	-108.44	-106.94	-105.24	-103.44	-102.04	-105.54	-108.04	-110.04	-115.54	-117.54
1.80	-114.44	-112.94	-111.24	-109.44	-108.04	-111.54	-114.04	-116.04	-121.54	-123.54
1.90	-120.44	-118.94	-117.24	-115.44	-114.04	-117.54	-120.04	-122.04	-127.54	-129.54
2.00	-126.44	-124.94	-123.24	-121.44	-120.04	-123.54	-126.04	-128.04	-133.54	-135.54
2.10	-132.44	-130.94	-129.24	-127.44	-126.04	-129.54	-132.04	-134.04	-139.54	-141.54
2.20	-138.44	-136.94	-135.24	-133.44	-132.04	-135.54	-138.04	-140.04	-145.54	-147.54
2.30	-144.44	-142.94	-141.24	-139.44	-138.04	-141.54	-144.04	-146.04	-151.54	-153.54
2.40	-150.44	-148.94	-147.24	-145.44	-144.04	-147.54	-150.04	-152.04	-157.54	-159.54
2.50	-156.44	-154.94	-153.24	-151.44	-150.04	-153.54	-156.04	-158.04	-163.54	-165.54
2.60	-162.44	-160.94	-159.24	-157.44	-156.04	-159.54	-162.04	-164.04	-169.54	-171.54
2.70	-168.44	-166.94	-165.24	-163.44	-162.04	-165.54	-168.04	-170.04	-175.54	-177.54
2.80	-174.44	-172.94	-171.24	-169.44	-168.04	-171.54	-174.04	-176.04	-181.54	-183.54
2.90	-180.44	-178.94	-177.24	-175.44	-174.04	-177.54	-180.04	-182.04	-187.54	-189.54
3.00	-186.44	-184.94	-183.24	-181.44	-180.04	-183.54	-186.04	-188.04	-193.54	-195.54
3.10	-192.44	-190.94	-189.24	-187.44	-186.04	-189.54	-192.04	-194.04	-199.54	-201.54
3.20	-198.44	-196.94	-195.24	-193.44	-192.04	-195.54	-198.04	-200.04	-205.54	-207.54
3.30	-204.44	-202.94	-201.24	-199.44	-198.04	-201.54	-204.04	-206.04	-211.54	-213.54
3.40	-210.44	-208.94	-207.24	-205.44	-204.04	-207.54	-210.04	-212.04	-217.54	-219.54
3.50	-216.44	-214.94	-213.24	-211.44	-210.04	-213.54	-216.04	-218.04	-223.54	-225.54
3.60	-222.44	-220.94	-219.24	-217.44	-216.04	-219.54	-222.04	-224.04	-229.54	-231.54
$\Delta OASPL$	0.000	1.500	3.200	5.000	6.400	2.900	0.400	-1.600	-4.054	-6.054

REPORT DOCUMENTATION PAGE		Form Approved OMB No. 0704-0188

1. REPORT DATE *(DD-MM-YYYY)*	2. REPORT TYPE	3. DATES COVERED *(From - To)*
01-08-2012	Technical Memorandum	

4. TITLE AND SUBTITLE
A Comparison of Combustor-Noise Models

5a. CONTRACT NUMBER

5b. GRANT NUMBER

5c. PROGRAM ELEMENT NUMBER

6. AUTHOR(S)
Hultgren, Lennart, S.

5d. PROJECT NUMBER

5e. TASK NUMBER

5f. WORK UNIT NUMBER
WBS 561581.02.08.03.45.02.01

7. PERFORMING ORGANIZATION NAME(S) AND ADDRESS(ES)
National Aeronautics and Space Administration
John H. Glenn Research Center at Lewis Field
Cleveland, Ohio 44135-3191

8. PERFORMING ORGANIZATION REPORT NUMBER
E-18346

9. SPONSORING/MONITORING AGENCY NAME(S) AND ADDRESS(ES)
National Aeronautics and Space Administration
Washington, DC 20546-0001

10. SPONSORING/MONITOR'S ACRONYM(S)
NASA

11. SPONSORING/MONITORING REPORT NUMBER
NASA/TM-2012-217671

12. DISTRIBUTION/AVAILABILITY STATEMENT
Unclassified-Unlimited
Subject Category: 71
Available electronically at http://www.sti.nasa.gov
This publication is available from the NASA Center for AeroSpace Information, 443-757-5802

13. SUPPLEMENTARY NOTES

14. ABSTRACT
The current status of combustor-noise prediction in the NASA Aircraft Noise Prediction Program (ANOPP) for current-generation (N) turbofan engines is summarized. Best methods for near-term updates are reviewed. Long-term needs and challenges for the N+1 through N+3 timeframe are discussed. This work was carried out under the NASA Fundamental Aeronautics Program, Subsonic Fixed Wing Project, Quiet Aircraft Subproject.

15. SUBJECT TERMS
Aeroacoustics; Turbomachinery noise; Core noise; Combustor noise

16. SECURITY CLASSIFICATION OF:			17. LIMITATION OF ABSTRACT	18. NUMBER OF PAGES	19a. NAME OF RESPONSIBLE PERSON
a. REPORT	b. ABSTRACT	c. THIS PAGE			STI Help Desk (email:help@sti.nasa.gov)
U	U	U	UU	33	19b. TELEPHONE NUMBER *(include area code)* 443-757-5802